(in Figure 6A or B) are larger than those of the Mn(II) complexes because of the increase of molecular asymmetry by introduction of chloride as the axial ligand. The considerable difference in the intensities of CD spectra between Mn(II) and Mn(III) complexes of $MnT_{men}PP$ or $MnT_{ben}PP$ did not reflect the same extent of the stereoselectivities between the Mn(II) and Mn(III) complexes possessing identical chiral parts (denoted as men or ben in Table V). The chirality of the L(-)-menthyl or D(+)-α-menthylbenzyl moiety of the porphyrin seems to directly influence their stereoselective abilities for the coordination of the substrate to the manganese chiral porphyrins, though the chiral substituents of these porphyrins are in the para positions of the TPP structures. The change in the chiral ligand of the three atropisomers of $Mn^{II}T_{cam}PP$ from the $\alpha,\alpha,\beta,\beta$-type to the $\alpha,\alpha,\alpha,\alpha$-one via the $\alpha,\alpha,\alpha,\beta$-one increased the intensities of the CD spectra at 440 nm (with a gradual decrease of the ellipticity at 460 nm) by changing the extent of molecular asymmetry around the central metal of the porphyrin (Figure 6C). Such a ligand change from the $\alpha,\alpha,\beta,\beta$-type to the $\alpha,\alpha,\alpha,\alpha$-one is not associated with the substrate stereoselectivity of $Mn^{II}T_{cam}PP$ having the identical L(-)-camphanoyl moiety; however, we assume that the appropriate orientation of the chiral L(-)-camphanoyl portion in $\alpha,\alpha,\alpha,\alpha$-$Mn^{II}T_{cam}PP$ for the coordination sites of the substrate would result in not only effective substrate stereoselection but also high enantiomeric excess of the ring-opening product via the Criegee rearrangement reaction.

Contribution from the Department of Chemistry, Princeton University, Princeton, New Jersey 08544, and Department of Chemistry, National Taiwan University, Taipei, Taiwan 10764, Republic of China

Resonance Raman and Magnetic Resonance Spectroscopic Characterization of the Fe(I), Fe(II), Fe(III), and Fe(IV) Oxidation States of Fe(2-TMPyP)$^{n+}$(aq)

Kenton R. Rodgers,† Robert A. Reed,† Y. Oliver Su,‡ and Thomas G. Spiro*,†

Received November 27, 1991

Four oxidation states of aqueous *meso*-5,10,15,20-tetrakis(2-*N*-methylpyridyl)porphinatoiron {Fe(2-TMPyP)(aq)} have been characterized at pH 9 and 12 via resonance Raman (RR), NMR, and ESR spectroscopic methods. These pH values were chosen because they are below and above the pK_a values of the Fe(II) (11.2), Fe(III) (11.0), and Fe(IV) (10.0) complexes. The 2-$TMPyP^{2+}$ ligand stabilizes four iron oxidation states, I–IV, in aqueous solution. The porphyrin core size marker band frequencies in the RR spectra are consistent with the metal ion radius increasing from Fe(IV) to Fe(II), but decreasing again for Fe(I). The Fe(I) core size is smaller than that of the Fe(II) species because Fe(I) is four-coordinate and low spin, whereas Fe(II) is five-coordinate and high spin. ESR data of the highly reduced complex ($g_\perp$ = 2.32 and $g_\parallel$ = 2.00) clearly demonstrate that Fe(II) reduction gives Fe(I) and not the porphyrin π-anion radical at pH 9 and 12. This is the first Fe(I) complex to be observed in aqueous solution, and the potentials of the Fe(II/I) couples (-0.740 V at pH 9 and -0.763 V at pH 12) are among the most positive of any yet observed for a porphinato complex. The first observation of a Fe^{II}–OH stretch in a model heme complex is reported and assigned to a band at 464 cm^{-1} on the basis of its 20-cm^{-1} downshift in $H_2{}^{18}O$. The Fe^{II}–OH adduct is five-coordinate and high spin on the basis of its RR and NMR spectra. The Fe(IV/III) potentials at pH 9 and 12 are among the least positive ever reported for porphyrin complexes. For solutions with pH > p$K_{a[Fe(IV)]}$, an Fe(IV) complex can be chemically or electrochemically generated and is stable for hours at room temperature. The low-frequency RR spectrum of this species exhibits an Fe^{IV}=O stretch at 763 cm^{-1}, which was assigned on the basis of its 31-cm^{-1} downshift in $H_2{}^{18}O$. This Fe(IV) complex gains its stability from coordination of the ferryl iron by an axial hydroxide ligand. For solutions with pH < p$K_{a[Fe(IV)]}$, a transient Fe(IV) species is generated. At both pH values, the Fe(IV) complexes are converted to porphyrin π-cation radical species at 120 K, as evidenced by their broad ESR lines near g = 2. However, the RR data indicate that an e_g ground state is thermally accessible and that the primary species in the room temperature solution is an Fe(IV) complex. The six-coordinate Fe(IV) species shows an upfield β-pyrrole ^2H NMR isotropic shift (-9.9 ppm) that is consistent with previously characterized six-coordinate porphinatoiron(IV) complexes in nonaqueous solution. Resonance Raman, NMR, and ESR data for the various oxidation states and states of axial ligation in the Fe(2-TMPyP) complexes suggest that the unique ability of this porphyrin ligand to stabilize both Fe(I) and Fe(IV) oxidation states is primarily due to the electrostatic influence of the *N*-methylpyridinium moieties at the porphyrin periphery, as opposed to perturbation of the interaction between metal ion and tetraarylporphyrin π orbitals. The stabilization of such a wide range of oxidation states is unprecedented in iron porphyrin chemistry and demonstrates that it is possible to modulate the coordination and redox chemistry of model hemes through variations in the electrostatic potential in which it resides without severely perturbing the intrinsic properties of the metalloporphine moiety.

Introduction

The rich chemistry exhibited by heme proteins has spawned numerous studies involving model heme complexes. These porphinato complexes have been employed as structural and reactivity models to relate heme structure and environment to reactivity, and to its control, as well as to tailor catalytic oxidants for synthetic purposes.

Two aspects of heme reactivity that are influenced by its protein environment are its oxidation/reduction potentials and the thermodynamics and kinetics of axial ligation. As axial ligand binding constants for the heme are nearly always a function of solution acidity or basicity, the axial coordination chemistry of aqueous porphinatoiron complexes with water and hydroxide ion is fundamental to understanding the coordination chemistry of aqueous heme proteins. Recent accounts from this laboratory reported the first observations of axial Fe^{III}–OH stretching vibrations in a model heme complex.[1] For solutions in which 5 < pH < 11, the principal species is the five-coordinate hydroxo-*meso*-5,10,15,20-tetrakis(2-*N*-methylpyridyl)porphinatoiron(III) [(Fe(2-TMPyP)$(OH)^{4+}$(aq)] complex, whereas at alkaline pH (pH > 11) the dominant species is the bis(hydroxo) species [Fe(2-TMPyP)$(OH)_2{}^{3+}$(aq)].[1] Recent work by Chen et al.[2] suggested that, as well as facilitating the formation of these monomeric hydroxoiron(III) complexes, the water-soluble porphyrin ligand in this complex exhibits the remarkable ability to stabilize Fe(I) and Fe(IV) in aqueous alkaline solution at ambient temperature. Moreover, the stabilities of most of these species are sufficient to permit their characterization via resonance Raman

* Author to whom correspondence should be addressed.
† Princeton University.
‡ National Taiwan University.

(1) (a) Reed, R. A.; Rodgers, K. R.; Kushmeider, K.; Su, Y. O.; Spiro, T. G. *Inorg. Chem.* **1990**, *29*, 2881. (b) Rodgers, K. R.; Reed, R. A.; Su, Y. O.; Spiro, T. G. *New J. Chem.*, in press.
(2) Chen, S.-M.; Sun, P.-J.; Su, Y. O. *J. Electroanal. Chem.* **1990**, *294*, 361.

0020-1669/92/1331-2688$03.00/0

(RR), NMR, and ESR spectroscopic investigations.

To date, all porphinatoferrate(I) complexes have been studied in scrupulously dry and anaerobic organic solvent systems.[3] Trace water contamination has always been a concern in the generation and physical characterization of these complexes due to the facile reduction of water by the Fe(I) species. However, the 2-TMPyP^{2+} ligand is sufficiently electron withdrawing to shift the potential of the Fe(II/I) couple anodic of that for water reduction, and it is thus possible to generate an Fe^{I}(2-TMPyP)$^{3+}$(aq) species.

The Fe(IV) complex in this study is stable for hours at pH 12. Such Fe(IV) stability has rarely been observed in heme model compound chemistry. Studies by Shedbalkar and co-workers[4a] and by Bell et al.[4b] represent the only other such obervations. These accounts report Fe(IV) complexes of a hematoporphyrin derivative[4a] and several tetraarylporphyinatoiron derivatives,[4b] respectively, that are stable on the order of hours at room temperature.

The present account constitutes an extension of our previous work and contains the detailed resonance Raman and magnetic resonance spectroscopic characterization of four oxidation states of the Fe(2-TMPyP)$^{n+}$(aq) complex.

Experimental Section

Synthesis. $H_2$2-TPyP was prepared via condensation of 2-pyridinecarboxaldehyde and pyrrole in propionic acid at ambient temperature. Methylation of the pyridyl nitrogens was carried out in neat dimethyl sulfate at 100 °C. Iron insertion was carried out under N_2 by adding solid $FeCl_2$ to a refluxing aqueous solution of $H_2$2-TMPyP. The resulting ferrous complex was oxidized by subsequent exposure to atmospheric oxygen. Fe(2-TMPyP)$(ClO_4)_5$ was then precipitated by dropwise addition of saturated aqueous $NaClO_4$.[5] The complex was twice recrystallized from water. The UV–visible spectrum of the product was consistent with that previously reported.[6] The analogous β-pyrrole deuterated compound {Fe(2-TMPyP-d_8)$(ClO_4)_5$} was prepared as described above with the following modification.[7] A mixture of 250 mL of propionic anhydride and 39.0 g of ^2H_2O was brought to reflux under Ar. When the hydrolysis reaction was complete (the solution was no longer biphasic), 6.0 mL of pyrrole was added to the propionic acid-d_1 and reflux was continued for 1 h under Ar. The slightly brown solution was then cooled to ambient temperature and opened to the air, and 8.2 mL of 2-pyridinecarboxaldehyde was added. This procedure afforded H_2TPyP-d_8, which was methylated, metalated, and isolated as described above. The product, $H_2$2-TMPyP-d_8, was determined to be 87.5% deuterated via integration of the 500-MHz proton NMR spectrum. The calculated extent of deuteration on the basis of the proportions of ^2H_2O and pyrrole used in the reaction was 90%. Hence, there was very little, if any back exchange of the β-pyrrole deuterons during the methylation and metalation reactions.

Reagents. Carbonate salts that were used in the preparation of buffers were analytical grade materials. $NaClO_4$ was twice recrystallized and dried under vacuum overnight at 100 °C. The water used in all spectroscopic and electrochemical experiments was distilled and deionized. Solution pH values were determined by use of a glass electrode and pH meter that were calibrated with standard buffers before each measurement.

Electrochemistry. Electrochemical studies were performed with a commercial potentiostat and potential programmer. Cyclic voltammetry (CV) and bulk electrolyses were carried out in a three-chamber cell in which the chambers were separated by medium-porosity glass frits. The scan rate for CV measurements was 50 mV/s. Potentials were measured versus the Ag/AgCl (saturated KCl) reference with a Pt wire serving as the counter electrode. The solution conditions at pH 9 were 0.1 M $NaClO_4$ and 0.1 M Na_2CO_3. We have demonstrated via acid–base titration, monitored by RR,[1a] that, although the second pK_a for Fe^{III}(2-TMPyP)(OH)$^{4+}$(aq) is slightly decreased in carbonate medium, the speciation of the hydroxide complexes as well as the Fe–OH frequencies remain the same as in perchlorate medium. Solution conditions at pH 12 were 0.2 M $NaClO_4$. For CV experiments, the working electrode was a glassy carbon disk. The electrode was polished and preconditioned by holding it at −1.5 V vs Ag/AgCl in 0.2 M $NaClO_4$ for 5 min. For bulk electrolyses, Pt gauze was employed as the working electrode. Electrolysis was continued until the cell current had fallen to less than 5% of its initial value. All of the electrochemical experiments were either carried out under N_2, under Ar in an inert atmosphere box, or in a septum-sealed cell that was purged with O_2-scavenged Ar. All potentials are reported versus Ag/AgCl (saturated KCl).

Resonance Raman Spectroscopy. Resonance Raman spectra were collected in the 135° backscattering configuration with *f*1.2 collection optics. Depolarization measurements were made using a photographic polarization filter between the collection lens and the *f*-matching lens. A polarization scrambler was also employed to preclude wavelength-sensitive spectrometer throughput artifacts due to polarization properties of the gratings. The sample was contained in a 5 mm spinning NMR tube or a stirred electrochemical cell. The scattered light was filtered and dispersed onto a 1024 diode array detector (maintained at −30 °C) with an *f*5.4 triple spectrometer. The excitation wavelengths used in these experiments were 413.1 nm (Kr^+ laser), 441.6 nm (HeCd laser), 457.9 nm (Ar^+ laser), and 465.8 nm (Ar^+ laser). The excitation wavelengths were chosen to maximize resonance enhancement of the Raman bands for the species under investigation. The Raman shifts are corrected for the index of refraction of air at their respective wavelengths and are, therefore, absolute Raman shifts (i.e. the reported Raman shifts are in vacuo and, therefore, independent of the excitation wavelength). Indene, carbon tetrachloride, and dimethylformamide were used as external references for spectral calibration.[8] Porphyrin concentrations were typically 1 mM.

NMR Spectroscopy. ^1H NMR spectra were carried out at 500 MHz in 5 mm diameter tubes. ^2H NMR spectra were acquired at 76.7 MHz or 38.4 MHz in 10 mm diameter tubes. Probe temperatures were measured directly by the method of Van Geet.[9] Porphyrin concentrations were typically 1 to 5 mM.

ESR Spectroscopy. ESR spectra were acquired at X-band frequency (9.35 GHz) and at 120 K. DPPH was employed as a $g = 2.002$ reference material. Electrochemically generated samples were prepared and sealed in an inert atmosphere glovebox, removed from the box, and immediately frozen in liquid N_2. Spectra typically contained 1024 data points. The scan rate and time constant were always chosen such that the product of scan rate (Gauss/s) and time constant (s) was much less than the smallest line width in the spectrum. The field modulation frequency was 100 kHz, and the modulation amplitude was 10 G. Porphyrin concentrations were typically 1 mM.

Results

Electrochemistry. The electrochemical behavior of the Fe(2-TMPyP)(aq) complexes has been reported by Chen et al.[9] The potentials reported herein are slightly different from those previously reported. This may be due to the fact that our potentials were determined in perchlorate medium, whereas Chen et al. used sulfate solutions. The following discussion of electrochemical results is presented as a basis for understanding the aqueous coordination chemistry of Fe(2-TMPyP)(aq) complexes as a function of pH.

Similar pK_a values are observed for the Fe(II), monohydroxoiron(III), and Fe(IV) species (11.2, 11.0, and 10.0, respectively),[1,2] and we have carried out our spectroscopic characterizations at pH 9 and 12 in order to ascertain the effects of the extent of hydroxide ligation on the stabilities and accessibilities of the high and low oxidation states discussed below. Figure 1 shows cyclic voltammograms (CVs) of Fe(2-TMPyP)$^{5+}$(aq) at pH 9 and 12. The CVs exhibit two quasi-reversible cathodic waves that correspond to the Fe(III/II) and Fe(II/I) couples. Both cathodic waves shift to more negative potentials when [OH^-] is increased, due to the need for one or more protons for reduction

(3) (a) Mashiko, T.; Reed, C. A.; Haller, K. J.; Scheidt, W. R. *Inorg. Chem.* **1984**, *23*, 3192. (b) Lexa, D.; Momenteau, M.; Rentien, P.; Gerard, R.; Saveant, J.-M.; Feng, X. *J. Am. Chem. Soc.* **1984**, *106*, 4755. (c) Srivatsa, G. S.; Sawyer, D. T.; Boldt, N. J.; Bocian, D. F. *Inorg. Chem.* **1985**, *24*, 2123. (d) Kadish, K. M.; Boisselier-Cocolios, B.; Simonet, B.; Chang, D.; Ledon, H.; Cocolios, P. *Inorg. Chem.* **1985**, *24*, 2148. (e) Lexa, D.; Saveant, J.-M.; Wang, D. L. *Organometallics* **1986**, *5*, 1428. (f) Teraoka, J.; Hashimoto, S.; Sugimoto, H.; Mori, M.; Kitagawa, T. *J. Am. Chem. Soc.* **1987**, *109*, 180. (g) Donohoe, R. J.; Atamian, M.; Bocian, D. F. *J. Am. Chem. Soc.* **1987**, *109*, 5593.

(4) (a) Shedbalkar, V. P.; Sandeep, M.; Samaresh, M. *J. Chem. Soc., Chem. Commun.* **1988**, 1238. (b) Bell, S. E. J.; Cooke, P. R.; Inchley, P.; Leanord, D. R.; Lindsey Smith, J. R. *J. Chem. Soc., Perkin Trans. 2* **1991**, 549.

(5) Davila, J.; Harriman, A.; Richouix, M.-C.; Milgrom, L. R. *J. Chem. Soc., Chem. Commun.* **1987**, 525.

(6) Kobayashi, N. *Inorg. Chem.* **1985**, *24*, 3324.

(7) Boersma, A. D.; Goff, H. M. *Inorg. Chem.* **1982**, *21*, 581.

(8) Absolute (in vaccuo) Raman shifts for these solvents were meticulously determined using lamp emission lines. This work was carried out in our laboratory by Dr. David Gosztola.

(9) Van Geet, A. L. *Anal. Chem.* **1970**, *42*, 679.

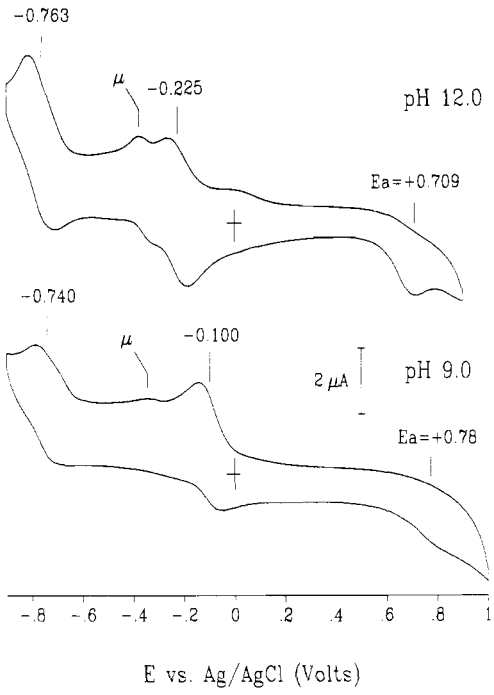

Figure 1. Cyclic voltammograms of $Fe(2\text{-}TMPyP)^{5+}(aq)$ at pH 9.0 and 12.0. The pH 9 solution was 0.1 M in ClO_4^- and 0.1 M in CO_3^{2-}, and the pH 12 solution was 0.2 M in ClO_4^-. Both solutions were 1 mM in $Fe(2\text{-}TMPyP)^{5+}(aq)$. "$\mu$" indicates reduction of μ-oxo dimer.

in alkaline solution. Figure 1 shows that in changing the pH from 9 to 12, potential of the Fe(III/II) couple shifts by −0.125 V (−0.100 V at pH 9 to −0.225 V at pH 12). The protonation and deprotonation reactions associated with Fe(III) and Fe(II) are (P = $2\text{-}TMPyP^{2+}$)[1,2]

$$Fe^{III}P(OH_2)^{5+}(aq) + H_2O \rightleftharpoons Fe^{III}P(OH)^{4+}(aq) + H_3O^+ \quad pK_{a1} = 4.71^1 \quad (1)$$

$$Fe^{III}P(OH)^{4+}(aq) + 2H_2O \rightleftharpoons Fe^{III}P(OH)_2^{3+}(aq) + H_3O^+ \quad pK_{a2} = 11.0^1 \quad (2)$$

$$Fe^{II}P(OH_2)^{4+}(aq) + H_2O \rightleftharpoons Fe^{II}P(OH)^{3+}(aq) + H_3O^+ \quad pK_a = 11.2^2 \quad (3)$$

These equilibria illustrate the effects of $[OH^-]$ upon the coordination chemistry of $Fe^{III}(2\text{-}TMPyP)^{5+}(aq)$ and $Fe^{II}(2\text{-}TMPyP)^{4+}(aq)$ and lead to the dependence of the Fe(III/II) couple upon pH. The reduction half-reactions in the pertinent pH ranges are

$$pH < pK_{a1[Fe(III)]} \quad Fe^{III}P(OH_2)^{5+} + e^- \rightleftharpoons Fe^{II}P(OH_2)^{4+} \quad (4)$$

$$pK_{a1[Fe(III)]} < pH < pK_{a2[Fe(III)]} \quad Fe^{III}P(OH)^{4+} + e^- + H_3O^+ \rightleftharpoons Fe^{II}P(OH_2)^{4+} + OH_2 \quad (5)$$

$$pK_{a2[Fe(III)]} < pH < pK_{a[Fe(II)]} \quad Fe^{III}P(OH)_2^{3+} + e^- + 2H_3O^+ \rightleftharpoons Fe^{II}P(OH_2)^{4+} + 3OH_2 \quad (6)$$

$$pH > pK_{a[Fe(II)]} \quad Fe^{III}P(OH)_2^{3+} + e^- + H_3O^+ \rightleftharpoons Fe^{II}P(OH)^{3+} + 2OH_2 \quad (7)$$

The observed potential difference of −0.125 V between pH 9 and 12 is less than the −0.189-V shift predicted on the basis of the 3-pH-unit change in pH. The discrepancy between predicted and observed potential shifts is attributed to differences in the electrode overpotential between the complexes at the two pH values, due to the corresponding variation in axial ligation of the metal ion.

The small wave at ~−0.37 V arises from a small amount of μ-oxo dimer that can be present at pH 9 and 12. As will be discussed below, the μ-oxo dimer can be hydrolyzed (cleaved) in acidic *and* alkaline solution.

A cathodic shift of 0.024 V is also observed in the potential of the Fe(II/I) couple between pH 9 and 12. If the Fe(I) species is four-coordinate, the only acid–base equilibrium that impacts on the potential of this couple is (3)

$$pH < pK_{a[Fe(II)]} \quad Fe^{II}P(OH_2)^{4+} + e^- \rightleftharpoons Fe^{I}P^{3+} + OH_2 \quad (8)$$

$$pH > pK_{a[Fe(II)]} \quad Fe^{II}P(OH)^{3+} + e^- + H_3O^+ \rightleftharpoons Fe^{I}P^{3+} + 2OH_2 \quad (9)$$

In this case, however, the potential should have shifted −0.047 V between pH 9 and 12. It is possible that OH^- binds to Fe(I) at high pH, thereby reducing the potential shift. The RR data suggest (see below) that the Fe(I) may be five-coordinate at pH 12. Alternatively, the lower observed potential shift may be due to differences in electrode overpotentials for reduction of the two different five-coordinate Fe(II) complexes. The CVs do show the Fe(II/I) couple to be less reversible at pH 9 than at pH 12, perhaps due to the proximity of the water reduction potential at pH 9, −0.730 V. At pH 12, the water potential, −0.907 V, is cathodically shifted by 0.144 V relative to that of the Fe(II/I) couple.

Anodic potential scans result in irreversible waves at pH 9 and 12. Figure 1 shows the potentials of the anodic waves (E_a), as the return cathodic wave is barely detectable at pH 12 and not discernible at pH 9. As with the reductive waves, there is a cathodic shift in the potential of E_a between pH 9 and 12. Equilibria 1 and 2 along with 10 illustrate the involvement of protons in the coordination chemistry of Fe(III) and Fe(IV) in our noncomplexing aqueous solutions. The anticipated shift in

$$Fe^{IV}OP^{5+}(aq) + 2H_2O \rightleftharpoons Fe^{IV}OP(OH)^{4+}(aq) + H_3O^+ \quad pK_a = 10.0^2 \quad (10)$$

the potential of the Fe(IV/III) couple is inferred from the redox couples shown below in the indicated pH ranges.

$$pH < pK_{a1[Fe(III)]} \quad Fe^{IV}OP^{4+} + e^- + 2H_3O^+ \rightleftharpoons Fe^{III}P(OH_2)^{5+} + 2OH_2 \quad (11)$$

$$pK_{a1[Fe(III)]} < pH < pK_{a[Fe(IV)]} \quad Fe^{IV}OP^{4+} + e^- + H_3O^+ \rightleftharpoons Fe^{III}P(OH)^{4+} + OH_2 \quad (12)$$

$$pK_{a[Fe(IV)]} < pH < pK_{a2[Fe(III)]} \quad Fe^{IV}OP(OH)^{3+} + e^- + 2H_3O^+ \rightleftharpoons Fe^{III}P(OH)^{4+} + 3OH_2 \quad (13)$$

$$pH > pK_{a2[Fe(III)]} \quad Fe^{IV}OP(OH)^{3+} + e^- + H_3O^+ \rightleftharpoons Fe^{III}P(OH)_2^{3+} + OH_2 \quad (14)$$

As one or more protons are involved in all of the Fe(IV/III) couples, the corresponding potential is always dependent on solution pH. The projected shift of −0.236 V is greater than the observed shift of ~−0.07 V for E_a (Figure 1). It is not surprising that the E_a values bear little relationship to the thermodynamic potentials.

The reversibility of the Fe(IV/III) couple at pH 9 is less than that at pH 12 (Figure 1). Unlike the Fe(II/I) couple, this dissimilarity cannot be attributed to the difference in the potential for water oxidation because, even though the water potential shifts cathodically at higher pH values, it remains anodic of the Fe(IV/III) potential between pH 9 and 12. The observed disparity in reversibility is explained in terms of differences in the propensity for disproportionation of the Fe(IV) species at the two pH values. Without a hydroxide ligand in the sixth axial position, the Fe(IV/III) potential is sufficiently anodic to cause disproportionation of the Fe(IV) to Fe(III) and an Fe(IV) π-cation radical species, which would rapidly oxidize water. Such mechanisms for generation of two-electron oxidized species have been offered for similar tetraarylporphyrin systems in organic solvents.[10] Hence, even though the potential for water oxidation is anodic of the observed E_a at pH 9, the formation of a highly oxidized species via disproportionation accounts for the poor reversibility.

All of the iron oxidation states accessible via cyclic voltammetry can be generated in bulk via electrolytic oxidation at a Pt gauze

(10) Groves, J. T.; Gilbert, J. A. *Inorg. Chem.* **1986**, *25*, 123.

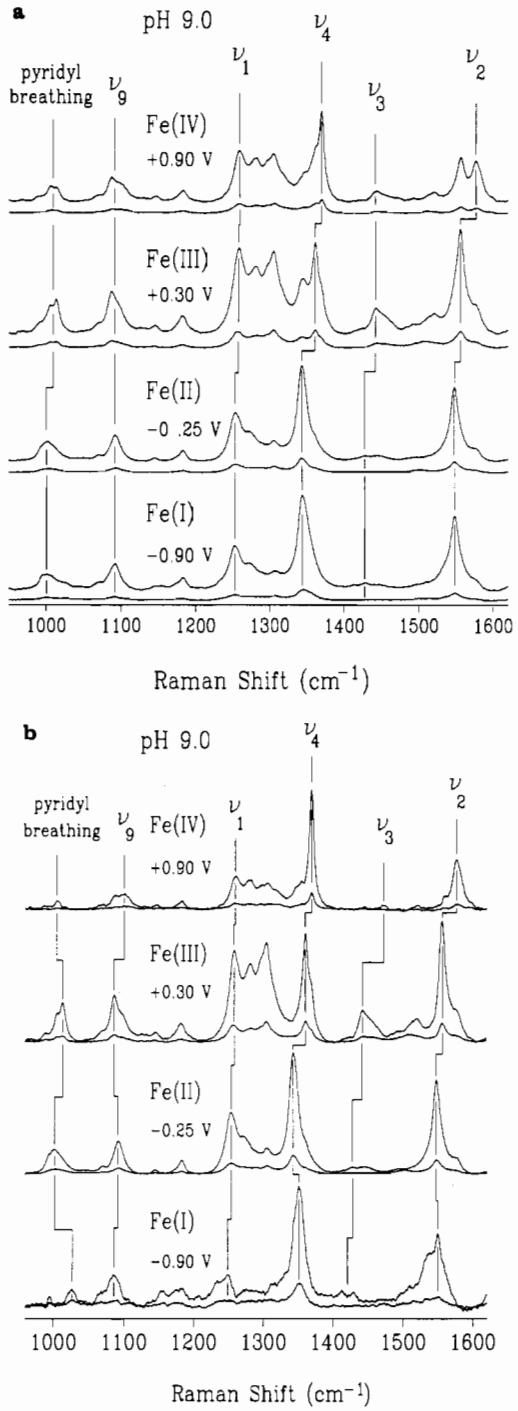

Figure 2. (A) Parallel and perpendicular high-frequency room-temperature resonance Raman spectra of Fe(2-TMPyP)$^{5+}$(aq) at pH 9.0 with 441.6-nm excitation: Fe(I), Fe(2-TMPyP)$^{5+}$(aq) electrolyzed at −0.90 V vs Ag/AgCl; Fe(II), Fe(2-TMPyP)$^{5+}$(aq) electrolyzed at −0.25 V; Fe(III), Fe(2-TMPyP)$^{5+}$(aq); Fe(IV), Fe(2-TMPyP)$^{5+}$(aq) electrolyzed at +0.90 V. Figure 2A contains the spectra as recorded. (B) Parallel and perpendicular high-frequency room-temperature resonance Raman spectra of Fe(2-TMPyP)$^{5+}$(aq) at pH 12.0 with 441.6-nm excitation: Fe(I), Fe(2-TMPyP)$^{5+}$(aq) electrolyzed at −0.88 V vs Ag/AgCl; Fe(II), Fe(2-TMPyP)$^{5+}$(aq) electrolyzed at −0.35 V; Fe(III), Fe(2-TMPyP)$^{5+}$(aq); Fe(IV), Fe(2-TMPyP)$^{5+}$(aq) electrolyzed at +0.70 V.

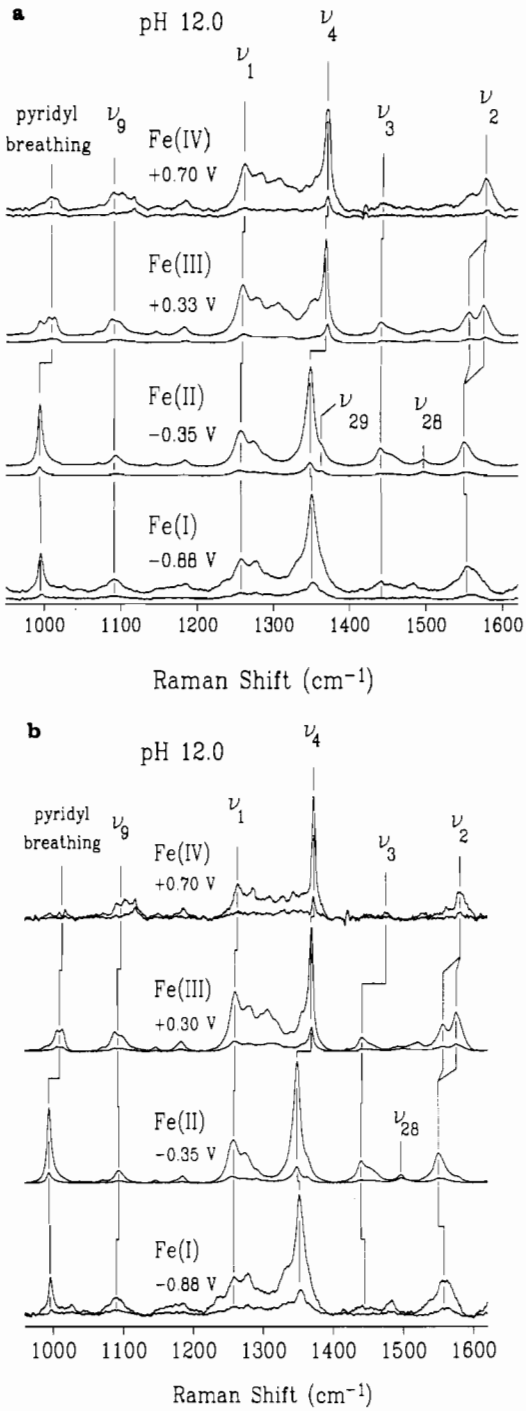

Figure 3. (A) Spectra from Figure 2a after the subtraction of contributions from other oxidation states, as described in the text. (B) Spectra from Figure 2b after the subtraction of contributions from other oxidation states.

electrode in a stirred cell. Moreover, at pH 12 the Fe(II) and Fe(IV) complexes were also generated using chemical reducing and oxidizing agents; ascorbate and hypochlorite were used in this study.

High-Frequency Resonance Raman Spectra. Figures 2 and 3 contain the 441.6-nm excited resonance Raman spectra of the four iron oxidation states discussed above. Figure 2 contains the spectra as they were collected, whereas Figure 3 contains spectra processed to reflect the spectra of the pure oxidation states. Inspection of Figure 2 reveals that the Fe(I) spectra strongly resemble those of Fe(II). This is due to the presence of some Fe(II), which exhibits higher scattering efficiency relative to Fe(I) due to its higher molar absorbtivity at the Raman excitation wavelength. Similarly, the ν_4 bands in the Fe(III) spectra clearly contain contributions from Fe(II) and Fe(IV). These bands are due to photoreduction and/or photodisproportionation of the Fe(III) complex in the laser beam, which are well documented characteristics of porphinatoiron(III) complexes.[11] We have confirmed this phenomenon experimentally, as the relative intensities show a clear dependence on laser power. Finally, the Fe(IV) spectra

(11) Peterson, M. W.; Rivers, D. S.; Richman, R. M. *J. Am. Chem. Soc.* **1985**, *107*, 2907.

Table I. Spectroscopic Data for Aqueous 2-TMPyP^{2+} Complexes of Fe(I), Fe(II), Fe(III), and Fe(IV) at pH 9.0

	Fe(I)	Fe(II)	Fe(III)	Fe(IV)
ν_1 (cm^{-1})	1249	1253	1259	1261
ν_2 (cm^{-1})	1550	1548	1556	1577
ν_3 (cm^{-1})	1422	1439	1443	
ν_4 (cm^{-1})	1352	1343	1361	1370
ν_9 (cm^{-1})	1086	1092	1087	1103
calcd core size (Å)[a]	2.016 ± 0.006	2.022 ± 0.006	1.999 ± 0.006	1.941 ± 0.006
β-pyrrole chemical shift (ppm)[b]		58.9	78.4	74.3
ESR g value[c]	2.32, 2.00	silent	5.68, 2.00	2.12
spin state	$^1/_2$	3	$^5/_2$	?

[a] Calculated core sizes based on the ν_2 frequencies. [b] Spectra acquired at ambient temperature. [c] Spectra acquired at −120 °C.

Table II. Spectroscopic Data for Aqueous 2-TMPyP^{2+} Complexes of Fe(I), Fe(II), Fe(III), and Fe(IV) at pH 12.0

	Fe(I)	Fe(II)	Fe(III)	Fe(IV)
ν_1 (cm^{-1})	1258	1257	1260	1265
ν_2 (cm^{-1})	1555	1549	1557, 1575	1581
ν_3 (cm^{-1})	1447	1440	1441	
ν_4 (cm^{-1})	1352	1349	1369	1373
ν_9 (cm^{-1})	1090	1094	1088, 1097	1103
calcd core size (Å)[a]	2.002 ± 0.006	2.019 ± 0.006	1.997, 1.946 ± 0.006	1.930 ± 0.006
β-pyrrole chemical shift (ppm)[b]		35.1	38.8, 40.3, 42.8	−1.0
ESR g value[c]	2.33, 2.01	silent	2.58, 2.16, 1.87	2.44
spin state	$^1/_2$	3	$^5/_2$, $^1/_2$	1

[a] Calculated core sizes based on the ν_2 frequencies. [b] Spectra acquired at ambient temperature. [c] Spectra acquired at −120 °C.

contain contributions from residual Fe(III). The presence of Fe(III) is evidenced by the shoulder on the ν_4 band, by the Fe(III) ν_2 band on the low-frequency side of the Fe(IV) ν_2 band at pH 9, and by the low-frequency shoulder on the Fe(IV) ν_2 band at pH 12. The spectra in Figure 3 were obtained from those in Figure 2 by interactively subtracting the spectra until the residual contributions to ν_2 and/or ν_4 were no longer discernible. The frequencies of the labeled bands in Figure 3 are listed in Tables I and II for pH 9 and 12, respectively.

The high frequency resonance Raman spectra in Figure 3 contain several bands that are sensitive to the porphyrin core size.[12] The core size is the projection of the metal–pyrrole nitrogen bond onto the mean square plane of the four pyrrole nitrogen atoms and is derived from single-crystal X-ray structures. Changes in oxidation state and spin state have measurable effects on the size of the porphyrin cavity and therefore on the frequencies of the core-size marker bands. As the porphyrin core is expanded, the porphyrin skeletal bonds are lengthened, and the core size marker bands generally shift to lower frequencies.[12] Figure 3 shows a stepwise decrease in the core-size marker frequencies, ν_2 (C_β–C_β stretch) and ν_4 (C_α–N stretch) between the 4+ and 2+ oxidation states of iron at both pH values. This is consistent with the increasing ionic radius of the metal ion in going from Fe(IV) to Fe(II). Previously reported core sizes and ν_2 frequencies were used to calculate the straight line that describes the correlation between these frequencies and the porphyrin core size (slope = $(2.8 \pm 0.2) \times 10^{-3}$, intercept = 6.3 ± 0.3).[12,13,14] The equation of this line along with our ν_2 frequencies (Table I and II) was used to calculate core sizes for our Fe(2-TMPyP)(aq) complexes. The ν_2 frequencies were chosen because they are the most reliable marker of core size in the 441.6-nm excited RR spectra (Figure 3). Although the ν_4 frequency does show a weak core size dependence, it is also sensitive to metal ion oxidation state and π-electron density.[15] Hence, in spite of ν_4 being the strongest band in the spectrum, ν_2 provides the more reliable indication of porphyrin core size.

The HOMO of metallotetraarylporphyrins has been shown to be the a_{2u} porphyrin π orbital.[16] The ν_2 frequency shifts down in TPP cation radicals[16c] because the nodal pattern for the a_{2u} porphyrin orbital makes it bonding with respect to the C_β–C_β bond, and removal of an electron from this orbital lowers the C_β–C_β bond order. Since ν_2 for the one-electron oxidation product of Fe(III) at pH 9 shifts *up*, it is concluded that the top RR spectra in parts a and b of Figure 3 (acquired at ambient temperature) are both associated with genuine Fe(IV) species.

The frequencies of the bands in the Fe(I) spectra (Figure 3, and Tables I and II) deviate from the above-mentioned correlation between oxidation state of the metal ion and the frequencies of the core-size marker bands. This deviation actually clarifies the assignment of this species as a genuine Fe(I) complex. The core size marker bands of an iron(II) porphyrin anion radical species would be expected to shift to *lower* frequencies since the electron would reside in an antibonding orbital and would lower the skeletal bond orders. This has been experimentally demonstrated in several laboratories, including ours, for ν_2 in [Zn(TPP)]$^{\bullet-}$, [Mg(TPP)]$^{\bullet-}$, and [Cu(TPP)]$^{\bullet-}$ complexes.[3f,3g,17–20] Hence, the slight upshifts that we observe for these marker bands upon one electron reduction

(12) (a) Parthasarathi, N.; Hanson, C.; Yamaguchi, S.; Spiro, T. G. *J. Am. Chem. Soc.* **1987**, *109*, 3865. (b) Spiro, T. G.; Strekas, T. C. *J. Am. Chem. Soc.* **1974**, *96*, 338.

(13) (a) Reed, C. A.; Mashiko, T.; Sheidt, W. R.; Spartalian, K.; Lang, G. J. *J. Am. Chem. Soc.* **1980**, *102*, 2302. (b) Cullen, D. L.; Meyer, E. F., Jr. *Acta Crystallogr., Sect. B* **1973**, *29*, 2507. (c) Hoard, J. L. In *Porphyrins and Metalloporphyrins*; Smith, K. M., Ed.; American Elsevier: New York, 1975; pp 317–376. (d) Hoard, J. L.; Scheidt, W. R. *Proc. Natl. Acad. Sci. U.S.A.* **1973**, *70*, 3919; **1974**, *71*, 1578. (e) Gonzalez, B.; Kouba, J.; Yee, S.; Reed, C. A.; Kirner, F. F.; Scheidt, W. R. *J. Am. Chem. Soc.* **1975**, *97*, 3247. (f) Mashiko, T.; Kastner, M. E.; Spartalian, K.; Scheidt, W. R.; Reed, C. A. *J. Am. Chem. Soc.* **1978**, *100*, 6354. (g) Kirner, J. F.; Garofollow, J., Jr.; Scheidt, W. R. *Inorg. Nucl. Chem. Lett.* **1975**, *11*, 107. (h) Scheidt, W. R.; Kastner, M. E.; Hatano, K. *Inorg. Chem.* **1978**, *17*, 706. (i) Hoard, J. L. *Science* **1971**, *174*, 295. (j) Radonovich, L. J.; Bloom, A.; Hoard, J. L. *J. Am. Chem. Soc.* **1972**, *94*, 2073. (k) Collins, D. M.; Countryman, R.; Hoard, J. L. *J. Am. Chem. Soc.* **1972**, *94*, 2066.

(14) The point for $Sn^{IV}(TPP)Cl_2$ was omitted in calculating the core sizes of our Fe[T9-2-*N*-MePy)P] complexes, as it deviated conspicuously from the frequency vs core size line for TPP^{2-} complexes.

(15) Spiro, T. G.; Li, X.-Y. In *Biological Applications of Raman Spectroscopy*; Spiro, T. G., Ed.; Wiley: New York, 1988; Vol. 3, Chapter 1.

(16) (a) Phillipi, M. A.; Goff, H. M. *J. Am. Chem. Soc.* **1982**, *104*, 6026. (b) Goff, H. M. In *Iron Porphyrins*; Lever, A. P. B.; Gray, H. B., Eds.; Addison-Wesley: Reading, MA, 1982; Part I, pp 237–281. (c) Czernuszewicz, R. S.; Macor, K. A.; Li, X.-Y.; Kincaid, J. R.; Spiro, T. G. *J. Am. Chem. Soc.* **1989**, *111*, 3860. (d) Spiro, T. G.; Czernuszewicz, R. S.; Li, X.-Y. *Coord. Chem. Rev.* **1990**, *100*, 541.

(17) Ksenofontova, N. M.; Maslov, V. G.; Sidorov, A. N.; Bobovich, Ya. S. *Opt. Spectrosc.* **1976**, *40*, 462.

(18) Reed, R. A.; Rodgers, K. R.; Spiro, T. G. *Unpublished results.*

(19) Yamaguchi, H.; Soeta, A.; Toeda, H.; Itoh, K. *J. Electroanal. Chem.* **1983**, *159*, 347.

(20) Scheer, H.; Inhoffen, H. H. In *The Porphyrin*; Dolphin, D., Ed.; Academic Press: New York, 1979; Vol. II, pp 45–90.

of Fe(2-TMPyP)(OH)$^{3+}$ and Fe(2-TMPyP)(OH$_2$)$^{4+}$ are inconsistent with ligand-centered reduction. The reduction of Fe(II) to Fe(I) is accompanied by a transition from high-spin Fe(II) to low-spin Fe(I) (see discussion of ESR data below). This removes an electron from the $d_{x^2-y^2}$ orbital, which decreases the Fe–N$_{pyrrole}$ bond distance and contracts the porphyrin core. Hence, the upshifts of core-size marker band frequencies in the Fe(I) spectra are consistent with assignment of the spectra to genuine Fe(I) complexes. The frequencies of the Fe(I) spectra (Tables I and II) show slightly higher frequencies at pH 12 than at pH 9. This may indicate five-coordination with an axial hydroxide ligand. Five-coordinate Fe(I) has been observed for Fe^{I}(TPP)$^-$ in pyridine solution[3g] and would be expected to shift the core size marker band frequencies up, as the metal ion would be pulled out of the plane of the porphine macrocycle, allowing it to contract.

The Fe(III) core-size marker band frequencies in Tables I and II are higher for the low-spin relative to the high-spin complex, as previously established for TPP complexes.[12] This is as expected, because the $d_{x^2-y^2}$ orbital, which is singly occupied with Fe–N$_{pyrrole}$ antibonding character in high-spin Fe(III), is empty in the low-spin species.[12]

Previously reported resonance Raman and magnetic resonance data have demonstrated that Fe(2-TMPyP)(OH)$_2^{3+}$(aq) solutions are in a thermal spin-state equilibrium comprised of $S = {}^1/_2$ and $S = {}^5/_2$ Fe(III). Raman spectroscopy provides a means of distinguishing between thermal spin-state equilibria and quantum mechanical spin admixtures by virtue of the vibrational time scale of the experiment. The latter gives rise to a single core size marker band, ν_2, at an intermediate frequency between the high- and low-spin bands, whereas the former exhibits a ν_2 band for each spin state.[12b] Figure 3 shows that at pH 12, the Fe^{III}(2-TMPyP)(OH)$_2^{3+}$(aq) spectrum clearly contains ν_2 bands for both spin states (see Tables I and II). Thus, the resonance Raman data demonstrate that the solution represents a thermal spin state equilibrium.[15] Although two ν_3 bands might also be expected in the spectrum of the spin-state mixture, this band is weak in the Soret-excited spectra and overlaps an unassigned band. Hence, interpretation of multiplicity in this band would be ambiguous.

Low-Frequency Resonance Raman Spectra. Fe^{IV}=O Modes. The Fe(IV) species, Fe^{IV}O(2-TMPyP)(OH)$^{3+}$(aq), Fe^{IV}O(2-TMPyP)(O^{2}H)$^{3+}$(aq), and Fe$^{IV}{}^{18}$O(2-TMPyP)(^{18}OH)$^{3+}$(aq) were generated via reaction with OCl$^-$ at room temperature, and Figure 4 shows the 441.6-nm-excited low-frequency RR spectrum before and after oxidation. The bands that correspond to the high- and low-spin Fe–OH stretching modes in the Fe(III) spectrum[1b] vanish upon OCl$^-$ addition, with the simultaneous appearance of a band at 763 cm^{-1}. The band(s) centered at 440 cm^{-1} in the Fe(IV) spectra in Figure 4 are attributed to porphyrin modes, as their frequencies do not exhibit isotope sensitivity. The 763-cm^{-1} band is assigned to the Fe^{IV}=O stretch in an oxohydroxoporphinatoiron(IV) complex on the basis of its the slight upshift in ^{2}H$_2$O and its 29-cm^{-1} downshift in H$_2{}^{18}$O. This isotope-shift pattern has been observed for the six-coordinate Mn^{IV}O(4-TMPyP)(OH)$^{3+}$(aq)[17] complex and is strongly suggestive of a six-coordinate oxohydroxoiron(IV) complex at pH 12. The slight upshift of the M=O frequency in ^{2}H$_2$O is attributed to a redistribution of the mode's potential energy. It has been shown that for Mn^{IV}O(4-TMPyP)(O^{2}H)$^{3+}$(aq), the trans M–O^{2}H stretch accounts for a higher fraction of the potential energy than the M–O–^{2}H bend (30% and 5%, respectively).[21] This is opposite from the relative potential energies in H$_2$O, wherein ν_{Mn-OH} accounts for 9% of the mode's potential energy and the Mn–O–^{1}H bend accounts for 16%. Although our upshift in ^{2}H$_2$O is small, it is suggestive of six-coordination in our Fe(IV) complex at pH 12. Furthermore, the Fe^{IV}=O ^{18}O-isotope shift of −29 cm^{-1} is very close to that for the six-coordinate oxohydroxomanganese(IV) analog (−27 cm^{-1}). This lends further support to the assignment

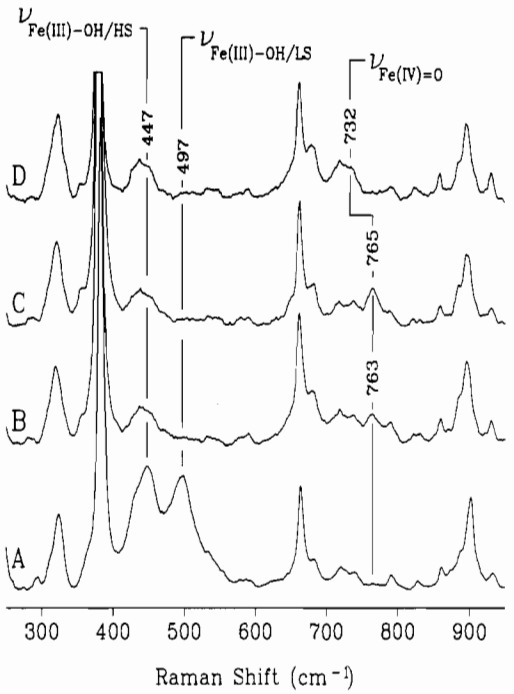

Figure 4. Low-frequency 441.6-nm excited RR spectra of (A) a mixture of high- and low-spin Fe^{III}(2-TMPyP)(OH)$_2^{3+}$(aq) at 0 °C, (B) solution from (A) after treatment with 1 equiv of OCl$^-$ in H$_2$O to generate Fe^{IV}O(2-TMPyP)(OH)$^{3+}$(aq), (C) Fe^{IV}O(2-TMPyP)(O^{2}H)$^{3+}$(aq) generated in ^{2}H$_2$O, and (D) Fe$^{IV}{}^{18}$O(2-TMPyP)(^{18}OH)$^{3+}$(aq) generated in H$_2{}^{18}$O.

of the pH 12 species to six-coordinate oxohydroxoiron(IV) complex.

Further evidence for hexacoordination in our pH 12 Fe(IV) complex lies in the low Fe=O stretching frequency. The frequency of the Fe^{IV}=O stretch for our oxoporphinatoiron(IV) complex is ca. 80 cm^{-1} lower than the Fe^{IV}=O stretches observed for five-coordinate FeO(TPP)[23] and FeO(TMP)[24] (852 and 841 cm^{-1}, respectively) and in the same frequency range as compound II for HRP,[25] myeloperoxidase,[26] and for CCP Compound ES[27] (787, 782, and 767 cm^{-1}, respectively). Although Compound ES of CCP is oxidized by two electrons above the ferric state of the enzyme, a recent crystal structure[28] along with mutagenesis/ESR data[29] indicates that the radical resides on a three-residue cluster that is about 10 Å from the heme plane. Insofar as the peroxidases contain a proximal imidazole with significant imidazolate character due to hydrogen bonding with residues in the proximal pocket,[30] these frequencies suggest that the Fe^{IV}O(2-TMPyP) species that gives rise to the 763-cm^{-1} Fe=O band is actually six-coordinate and contains a basic axial ligand trans to the ferryl oxygen. This correlation is borne out in a model compound study involving V^{IV}O(4-TMPyP)(OH$_2$)$^{4+}$(aq) and V^{IV}O(4-TMPyP)(OH)$^{3+}$(aq) wherein the V^{IV}=O stretching frequency is 60 cm^{-1} lower in the

(21) Czernuszewicz, R. S.; Su, Y. O.; Stern, M. K.; Macor, K. A.; Kim, D.; Groves, J. T.; Spiro, T. G. *J. Am. Chem. Soc.* **1988**, *110*, 4158.
(22) Su, Y. O.; Czernuszewicz, R. S.; Miller, L. A.; Spiro, T. G. *J. Am. Chem. Soc.* **1988**, *110*, 4150.
(23) Bajdor, K.; Nakamoto, K. *J. Am. Chem. Soc.* **1984**, *106*, 3045.
(24) Czernuszewicz, R. S.; Macor, K. A. *J. Raman Spectrosc.* **1988**, *19*, 553.
(25) (a) Terner, J.; Sitter, A. J.; Reczek, C. M. *Biochim. Biophys. Acta* **1985**, *828*, 73. (b) Oertling, W. A.; Babcock, G. T. *Biochemistry* **1988**, *27*, 3331.
(26) Oertling, W. A.; Hoogland, G.; Babcock, G. T.; Wever, R. *Biochemistry* **1988**, *27*, 5395.
(27) Hashimoto, S.; Teraoka, J.; Inubushi, T.; Yonetani, T.; Kitagawa, T. *J. Biol. Bhem.* **1986**, *261*, 11110.
(28) Edwards, S. L.; Xuong, N.; Hamlin, R. C.; Kraut, J. *Biochemistry* **1987**, *26*, 1503.
(29) (a) Sivaraja, M.; Goodin, D. B.; Smith, M.; Hoffman, B. M. *Science* **1989**, *245*, 738. (b) Fishel, L. A.; Villafranca, J. E.; Mauro, J. M.; Kraut, J. *Biochemistry* **1987**, *26*, 351. (c) Goodin, D. B.; Mauk, A. G.; Smith, M. *Proc. Natl. Acad. Sci. U.S.A.* **1986**, *83*, 1295.
(30) (a) Dunford, H. B.; Stillman, J. S. *Coord. Chem. Rev.* **1976**, *19*, 187. (b) Morrison, M.; Schonbaum, G. R. *Annu. Rev. Biochem.* **1976**, *45*, 861. (c) Hewson, W. D.; Hager, L. P. In *The Porphyrins*; Dolphin, D., Ed.; Academic Press: New York, 1979; Vol. VII, pp 295–332. (d) Dunford, H. B. *Adv. Inorg. Biochem.* **1982**, *4*, 41.

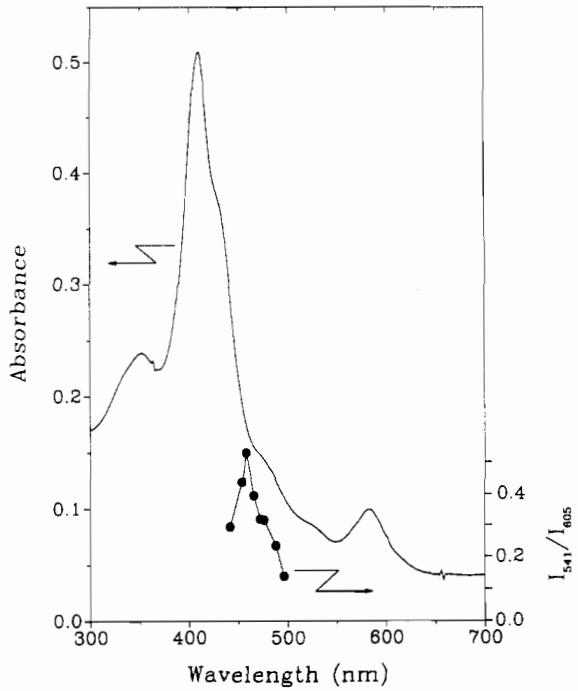

Figure 5. Electronic absorption spectrum of 5 μM Fe^{III}(2-TMPyP)-$(OH)^{4+}$(aq) at pH 9 and the resonance Raman excitation profile of the 541-cm^{-1} Fe^{III}–OH stretching band (●). The 605-cm^{-1} band of sodium cacodylate was used as an internal intensity standard. Wavelengths at which RR intensities were measured are 441.6, 454.5, 457.9, 465.8, 472.2, 476.5, 488.0, and 496.5 nm.

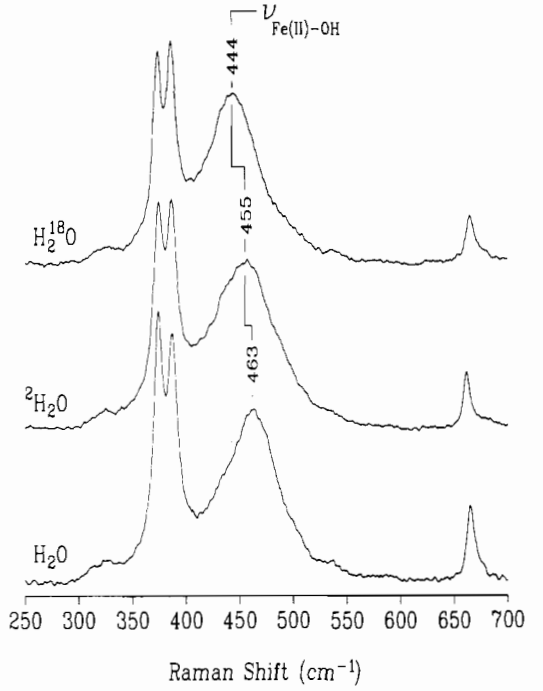

Figure 6. Low-frequency 413.1-nm excited RR spectra of Fe^{II}(2-TMPyP)$(OH)^{3+}$(aq) at pH 13 in the indicated solvents.

six-coordinate oxohydroxo- complex than in the oxoaquovanadium(IV) complex.[22]

Fe^{III}–OH Modes. The Fe^{III}–OH modes are strongly resonance enhanced in the 2-$TMPyP^{2+}$ complexes,[1] but efforts in this laboratory to observe this mode in Fe^{III}(TMP)OH have been unsuccessful. An understanding of this apparent inconsistency may be found in the excitation profiles of the various Fe^{III}–OH stretching bands. The low-frequency RR spectra of Fe^{III}(2-TMPyP)$(OH)_n^{(4-n)+}$(aq) along with the excitation profiles (EPs) of high- and low-spin Fe^{III}(2-TMPyP)$(OH)_2^{3+}$(aq) have been reported.[1] The EP of $\nu_{LS/Fe-OH}$ peaks just to the blue of the Soret absorption (presumably due to the selective enhancement by the $0 \rightarrow 1$ transition of the Soret band) from which it draws its enhancement, whereas the $\nu_{HS/Fe-OH}$ EP peaks near 485 nm and is likely enhanced via a z-polarized porphyrin-to-metal charge transfer transition [$\pi(a_{2u}) \rightarrow d_{x^2}(a_{1g})$] for which $\lambda_{max} \approx 484$ nm.[1b] Soret enhancement of the low-spin symmetric HO–Fe^{III}–OH vibration is likely due to coupling of the z electronic polarizability to the in-plane Soret electronic transition through π-interaction between the two axial hydroxide ligands and the iron d_π orbitals.[31] Soret enhancement of the Fe^{III}–OH vibrations is lost or at least greatly diminished for the five- and six-coordinate high-spin complexes, suggesting that the π-interaction responsible for Soret enhancement in the low-spin complex is also diminished. Thus, on the basis of these observations and rationalizations, Soret enhancement of the Fe^{III}–OH vibration in the high-spin Fe^{III}-(TMP)OH complex is not expected, and the charge transfer transitions may be at a different wavelength due to the altered porphyrin substituents.

The electronic absorption spectrum of the high-spin monohydroxo complex, Fe^{III}(2-TMPyP)$(OH)^{4+}$(aq), along with its excitation profile are shown in Figure 5. The 442-nm EP maximum is distinctly below the Soret absorption maximum and suggests the presence of a charge-transfer band. Again, the z-polarized $\pi(a_{2u}) \rightarrow d_{z^2}(a_{1g})$ charge transfer transition[31] is a likely candidate for the resonance enhancement of the Fe^{III}–OH stretch. Ligand-to-metal charge transfer transitions involving the axial hydroxide ligand(s) are also candidates for enhancement of the high-spin Fe^{III}–OH stretches.[15]

The Fe^{II}–OH Mode. Low-frequency RR spectra of Fe^{II}(2-TMPyP)$(OH)^{3+}$(aq) in H_2O, ^2H_2O, and $H_2{}^{18}O$ are shown in Figure 6. The spectrum in H_2O contains a broad band at 464 cm^{-1} that shifts down by 9 cm^{-1} in ^2H_2O and by 20 cm^{-1} in $H_2{}^{18}O$. This ^{18}O shift is accurately modeled by a diatomic oscillator with point masses of 56 and 17 amu. The ^2H shift is slightly less than that predicted using the two-point-mass model. A similar and previously modeled anomaly in the ^2H shift of the five-coordinate high-spin Fe^{III}–OH complex suggests that an isotope-sensitive fraction of the Fe^{II}–OH potential energy is accounted for by an Fe^{II}–O–H bend.[1a] Nevertheless, these isotope shifts (especially the ^{18}O shift) demonstrate that the 464-cm^{-1} band (Figure 6) is associated with the Fe^{II}–OH stretching mode. To the best of our knowledge, this is the first report of an iron(II)–hydroxide stretching vibration. The frequency of the high-spin Fe^{II}–OH mode is considerably lower than that of the high-spin five-coordinate Fe^{III}–OH mode (541 cm^{-1}). Although the occupancy of the metal ion σ and π orbitals that interact with the hydroxide ligand is the same for both iron oxidation states, the decrease in the Coulombic interaction between the 2+ metal ion and the hydroxide ion gives rise to the decrease in the frequency of the Fe^{II}–OH band relative to its Fe(III) counterpart.

As illustrated by the Fe^{II}–OH EP and the Fe(II) absorption spectrum in Figure 7, the EP of this band tracks the Soret absorption. As is the case with the low-spin HO–Fe–OH stretching mode, it is not possible to unambiguously elucidate the enhancement mechanism for this band because any charge transfer candidates that might be under the Soret would be obscured in the solution electronic absorption spectrum. However, it has been unambiguously demonstrated that the Fe–ImH vibration in Mb is enhanced via the in-plane porphyrin π–π^* (Soret) transition.[32] Thus, charge-transfer enhancement of the Fe^{II}–OH vibration is unlikely.

NMR Spectra. Figures 8 and 10 contain ^2H NMR spectra of the Fe(II), Fe(III), and Fe(IV) complexes of 2-$TMPyP^{2+}$-d_8 (selectively deuterated at the β-pyrrole carbons). These spectra contain resonances only from the β-pyrrole deuterons and natural abundance HDO, thereby simplifying interpretation of the spectra.

(31) Spiro, T. G. In *Iron Porphyrins*; Lever, A. P. B., Gray, H. B., Eds.; Addison-Wesley: Reading, MA, 1982; Part II, pp 89–159.

(32) Bacharoenpaurpong, O.; Schomacker, K. T.; Campion, P. M. *J. Am. Chem. Soc.* **1984**, *106*, 5688.

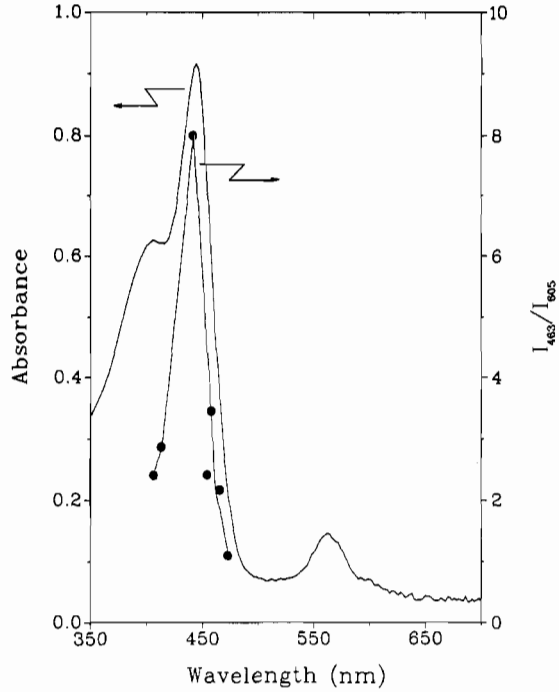

Figure 7. Electronic absorption spectrum of 5.6 μM Fe^{II}(2-TMPyP)-$(OH)^{3+}$(aq) and resonance Raman excitation profile of the 463-cm^{-1} Fe^{II}–OH stretching band (●). The 605-cm^{-1} band of sodium cacodylate was used as an internal intensity standard. Wavelengths at which RR intensities were measured are 406.7, 413.1, 441.6, 454.5, 457.9, 465.8, and 427.7 nm.

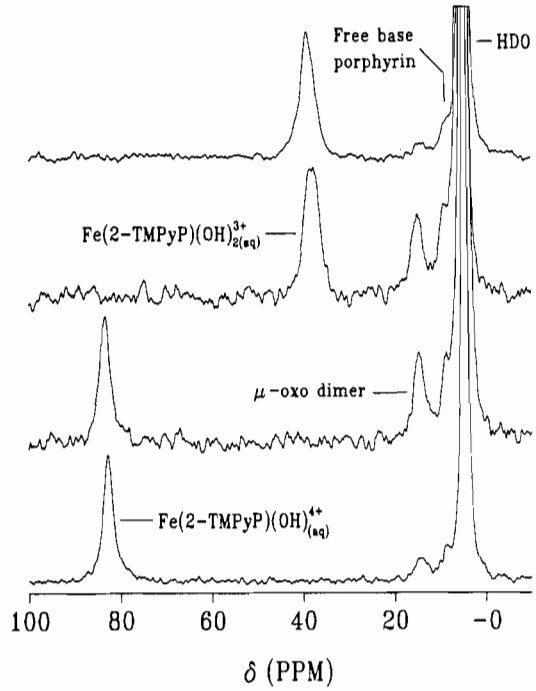

Figure 8. Room temperature 38.4-MHz ^2H NMR spectra of (A) 0.7 mM Fe^{III}(2-TMPyP-d_8)$(OH)^{4+}$(aq) at pH 6, (B) solution from (A) after refluxing for 20 min, (C) solution from (B) after raising the pH from 6 to 12 at room temperature, and (D) solution from (C) after refluxing for 45 min.

Furthermore, the smaller gyromagnetic ratio of ^2H relative to ^1H is manifested in a narrowing of the ^2H lines for paramagnetic molecules.[33] Spectra of the Fe(I) complex are not shown, as its low solubility precluded acquisition of useful NMR spectra.

(33) Swift, T. J. In *NMR of Paramagnetic Molecules*; La Mar, G. N., Horrocks, W. D., Holm, R. H., Eds.; Academic Press: New York, 1973; pp 53–83.

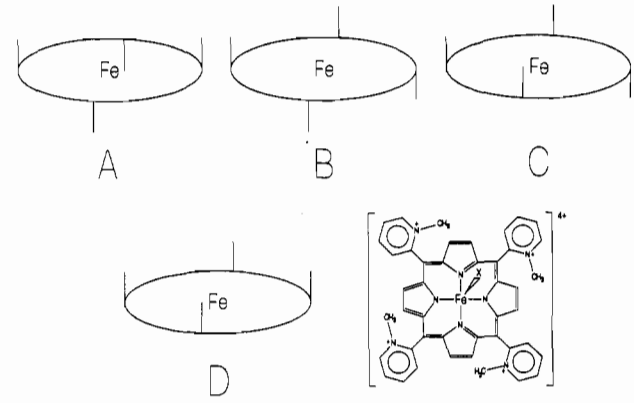

Figure 9. Illustration of the three non-μ-oxo dimer forming *N*-methylpyridyl rotational atropomers of Fe(2-TMPyP) and the one isomer that is able to dimerize. The 2-*N*-methylpyridyl moieties are out of the plane of the porphine macrocycle, with the *N*-methyl moiety oriented up or down as indicated for each atropomer.

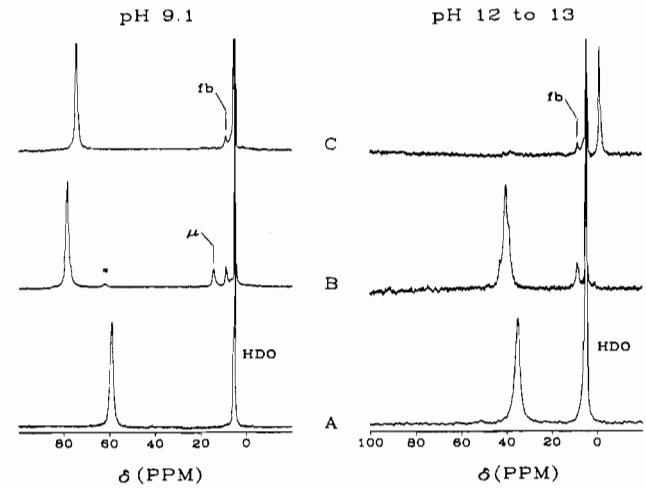

Figure 10. ^2H NMR spectra of the various oxidation states of Fe(2-TMPyP)$^{n+}$ at pH 9.1 and pH 12 to 13, respectively: (A) Fe(2-TMPyP-d_8)$(OH_2)^{4+}$(aq) (76.7 MHz, 295 K) and Fe(2-TMPyP-d_8)-$(OH)^{3+}$(aq) (38.4 MHz, 293 K); (B) Fe(2-TMPyP-d_8)$(OH)^{4+}$(aq) (76.7 MHz, 295 K) and Fe(2-TMPyP-d_8)$(OH)_2^{3+}$(aq) (38.4 MHz, 293 K); (C) Fe(2-TMPyP-d_8)$(OH)_n^{(5-n)+}$(aq) (76.7 MHz, 295 K) and FeO(2-TMPyP-d_8)$(OH)^{3+}$(aq) (76.7 MHz, 295 K).

The β-pyrrole deuteron shift of the singly reduced Fe(III) complex at pH 9.1 is 59.0 ppm (Table I) at 295 K. This is similar to the corresponding shifts for the five-coordinate high-spin Fe^{II}(TPP)(2-MeIm) (52.3 ppm vs TMS at 298 K) and [Fe^{II}-(TPP)(SR)]$^-$ (61.2 ppm vs TMS at 297 K) complexes.[34] The shift for our aqueous 2-$TMPyP^{2+}$ species at pH 12 is 35.0 ppm at 291 K (Table II) compared to 32.8 ppm for [Fe^{II}(TPP)OH]$^-$.[35] These consistencies between the NMR spectra of our Fe(II) complexes and those of previously characterized porphinatoiron(II) complexes further support the assignment of the high-pH species as a five-coordinate hydroxoporphinatoiron(II) complex and is consistent with the assignment of the pH 9.1 species as a five-coordinate high-spin aquoporphinatoiron(II) complex. These assignments are also consistent with the previous observation by Chen et al. of a single acid–base transition in the Fe(III/II) potential at pH 11.2.[2]

Figure 8 shows that heating a solution of the Fe(III) complexes induces formation of μ-oxo dimer at pH 6 and its cleavage at pH 12. The 14 ppm resonance is characteristic of the spin-coupled μ-oxo dimer.[36] This resonance is weak for a pH 6 solution at

(34) (a) Goff, H. M.; La Mar, G. N. *J. Am. Chem. Soc.* **1977**, *99*, 6599. (b) Mispelter, J.; Momenteau, M.; Lhoste, J. M. *Chem. Phys. Lett.* **1978**, *57*, 405. (c) Parmely, R. C.; Goff, H. M. *J. Inorg. Biochem.* **1980**, *12*, 269. (d) Lukat, G. S.; Goff, H. M. *Biochim. Biophys. Acta* **1990**, *1037*, 351.

(35) Shin, K.; Kramer, S. K.; Goff, H. M. *Inorg. Chem.* **1987**, *26*, 4103.

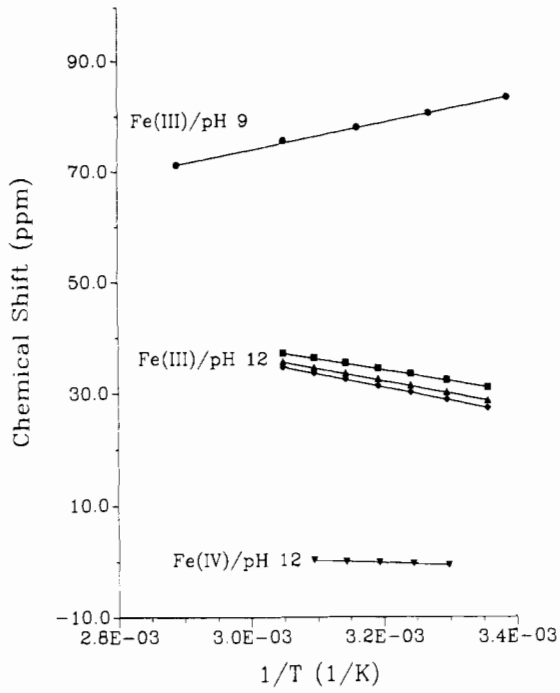

Figure 11. Curie plots for $Fe^{III}(2\text{-}TMPyP)(OH)^{4+}(aq)$ (38.4 MHz), $Fe^{III}(2\text{-}TMPyP)(OH)_2^{3+}(aq)$ (76.7 MHz), and $Fe^{IV}O(2\text{-}TMPyP)(OH)^{3+}(aq)$ (76.7 MHz).

room temperature (trace A) but becomes strong after refluxing for 20 min (trace B). The 83 ppm resonance arises from the dominant monohydroxo complex at pH 6. Integration gives a lower limit of 40% conversion to the μ-oxo dimer upon refluxing, but the actual conversion is higher, since the dimer is less soluble than the monomeric complexes, and precipitates from solution. The resulting dilution is reflected in the diminished S/N in trace B. We attribute the heating effect to equilibration of the four atropisomers shown in Figure 9. The thermodynamic stability of the μ-oxo dimer pulls the equilibrium toward isomer D, which does not inhibit dimerization because all four *N*-methyl groups are pointed to one side of the porphyrin plane.

When the pH of the previously refluxed solution is raised to pH 12 (trace C), the dimer peak is undiminished, while the monohydroxo peak is converted to a complex resonance at 40 ppm (see below) due to formation of the bis(hydroxide) complex. After the pH 12 solution is refluxed for 45 min, however (trace D), the 14 ppm peak nearly disappears and the S/N increases back to that observed initially in trace A, as the precipitated dimer redissolves. We conclude that the dimer is thermodynamically *unstable*, relative to the bis(hydroxo) complex at pH 12. Heating is necessary to overcome a kinetic barrier to hydrolysis of the μ-oxo bridge.

The Fe(III) spectrum at pH 9 exhibits a β-pyrrole chemical shift of 78.4 ppm, which is typical of five-coordinate high-spin porphinatoiron(III) complexes.[36] At pH 12, however, the spectrum displays some complexities. The β-pyrrole resonance exhibits multiplicity that is not apparent in the pH 9 spectrum (see Figure 10 and Table II). The ~40 ppm β-pyrrole-^{2}H envelope contains three components that arise from the three non-μ-oxo-dimer-forming rotational atropisomers shown in Figure 9. The relative intensities of the three peaks are very close to 4:8:2, which corresponds to the expected statistical populations of the B, C, and A atropisomers, respectively. As seen by the negative slopes of the Fe(III)/pH 12 Curie plots in Figure 11, the components of the 40 ppm envelope exhibit inverse Curie behavior. These data indicate that the $Fe^{III}(2\text{-}TMPyP)(OH)_2^{3+}(aq)$ complex is not a pure spin state at noncryogenic temperatures and is consistent with the simultaneous observation of ν_2 for high- and low-spin Fe(III) in the RR spectrum of $Fe^{III}(2\text{-}TMPyP)(OH)_2^{3+}(aq)$ (Figure 3). On the basis of typical high- and low-spin β-pyrrole shifts of 80 and −30 ppm, respectively,[36] we estimate that the 40 ppm envelope represents a 34/66 mixture of low- and high-spin $Fe^{III}(2\text{-}TMPyP)(OH)_2^{3+}(aq)$, respectively. Thus, the energy difference between the $S = {}^1/_2$ and $S = {}^5/_2$ states of $Fe^{III}(2\text{-}TMPyP)(OH)_2^{3+}(aq)$ is approximately kT at ambient temperature. In contrast to the shift of the pH 12 β-pyrrole-^{2}H envelope in Figure 10, the Curie plots corresponding to the pH 12 Fe(III) β-pyrrole resonances in Figure 11 indicate a room-temperature chemical shift for the β-pyrrole-^{1}H envelope centered at ~30 ppm. The Fe(III)/pH 12 Curie plots in Figure 11 were generated using shifts from ^{1}H spectra that were acquired in ^2H_2O. The center of the β-pyrrole deuteron envelope in Figure 10 is ~40 ppm in H_2O at room temperature, approximately 10 ppm farther downfield than the proton resonance in ^2H_2O. This difference in chemical shift suggests that the axial ligand field of the bis(hydroxo) complex is stronger in ^2H_2O than in H_2O, presumably due to H-bond effects, since the shift to higher field (in the direction of a pure low-spin complex[36]) indicates a greater low-spin population.

Inasmuch as the monomeric five-coordinate high-spin hydroxo complex exhibits a single β-pyrrole proton or deuteron resonance in the respective NMR spectra, the different rotational dispositions of the 2-*N*-methylpyridyl groups do not in themselves produce a measurable affect on the extent of σ-spin delocalization over the porphyrin macrocycle.[36] Assuming a similar insensitivity in the extent of π-spin delocalization in the low-spin complex, the three peaks observed in the bis(hydroxo) NMR spectrum are suggested to arise from variations in the relative high- and low-spin Fe(III) populations for the different atropisomers. This variation could reflect slightly differing ligand field strengths due to variations in the interaction of the OH^- ligands with the peripheral positive charges. In this interpretation, atropisomer B (Figure 9) feels the strongest ligand field, as evidenced by its tendency toward the low-spin β-pyrrole shift, whereas A experiences the weakest ligand field of the three non-μ-oxo dimer forming atropisomers.

A recently reported ^{1}H NMR spectrum of $Fe^{III}(4\text{-}TMPyP)(OH)_2^{3+}(aq)$ contains a single β-pyrrole proton resonance at 62 ppm in ^2H_2O at 298 K.[37] The temperature dependence of this β-pyrrole shift was not reported. We have examined the temperature dependence of the isotropic shift of this resonance at pH 12 and, like the $2\text{-}TMPyP^{2+}$ analog (see Figure 11), the Curie plot exhibits a *negative* slope. Hence, it is likely that the $Fe^{III}(4\text{-}TMPyP)(OH)_2^{3+}(aq)$ complex also exists in a thermal high-spin, low-spin equilibrium. The position of this average β-pyrrole resonance is closer to that of the pure high-spin Fe(III) and indicates a lower fraction of low-spin Fe(III) (16%) relative to the $2\text{-}TMPyP^{2+}$ derivative at room temperature. This decrease in low-spin population can be attributed to a weaker axial ligand field, because of the greater distance from the OH^- ligands to the peripheral charges on $4\text{-}TMPyP^{2+}$. The observation of a single β-pyrrole proton resonance is consistent with the above explanation of the three β-pyrrole resonances in the NMR spectrum of the $2\text{-}TMPyP^{2+}$ analog.

The top spectra in Figure 10 correspond to the one-electron oxidation products of $Fe^{III}(2\text{-}TMPyP)(OH)^{4+}(aq)$ and $Fe^{III}(2\text{-}TMPyP)(OH)_2^{3+}(aq)$ at pH 9 and 12, respectively. At pH 9, the NMR spectrum contains a single β-pyrrole resonance at 74.3 ppm that is probably an average signal from Fe(III) and a residual amount of Fe(IV). The high reactivity of the high-valent species at pH 9 makes it impossible to acquire an NMR spectrum of the pure high-valent complex at room temperature. The diminished isotropic shift relative to the pure five-coordinate high-spin Fe(III) complex indicates that the Fe(III) and high-valent complexes are in rapid electron exchange on the 77-MHz time scale. The observation of a diminished shift relative to the pure high-spin Fe(III) complex is not inconsistent with the formation of Fe(IV) at room temperature as concluded on the basis of the RR spectrum. It

(36) La Mar, G. N.; Walker, F. A. In *The Porphyrins*; Dolphin, D., Ed.; Academic Press: New York, 1979; Vol. IV, Chapter 2.

(37) Ivanca, M. A.; Lappin, A. G.; Scheidt, W. R. *Inorg. Chem.* **1991**, *30*, 711.

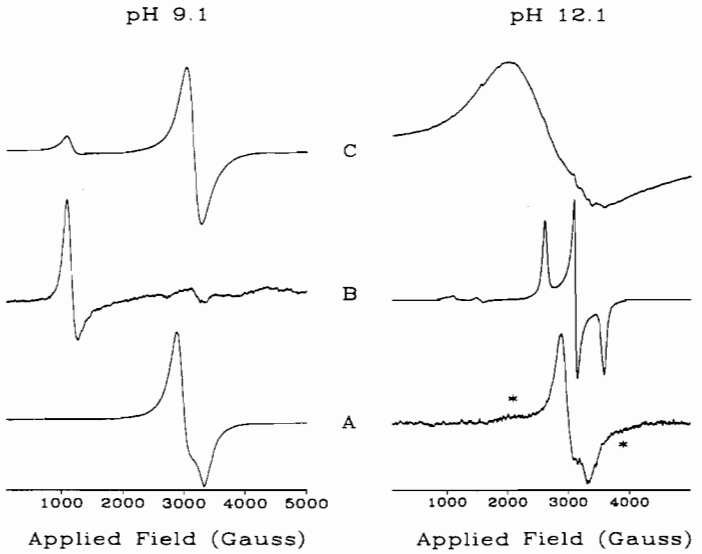

Figure 12. −120 °C X-band ESR spectra of the Fe(I) (A) and Fe(III) (B) complexes of 2-TMPyP^{2+}, and the one-electron oxidation product of Fe(III) (C) at pH 9.1 and pH 12.0. The asterisks on spectrum A at pH 12 indicate intensity from a small amount of what is likely Fe^{I}(2-TMPyP)(OH)$^{2+}$(aq) (see text). Spectral acquisition parameters were as described in the Experimental Section.

is interesting to note that the ^{1}H NMR spectrum reported by Bell et al. for the Fe^{IV}O(4-TMPyP)(OH$_2$)$^{4+}$(aq) complex contains a β-pyrrole proton resonance at 10 ppm. As is the case for our pH 9 spectrum, the sign of this isotropic shift is opposite of what is expected for a low-spin (S = 1) tetraarylporphinatoiron(IV) complex. The unpaired spins of the paramagnetic metal center are in orbitals of π symmetry (d_{xz} and d_{yz}). The contact shift of the β-pyrrole protons is, therefore, expected to be dictated via a π spin-delocalization mechanism, which is known to elicit β-pyrrole isotropic shifts to higher field in TPP-type porphyrins.[36] The observation of a slight downfield shift is consistent with our ^{2}H NMR observation at pH 9 and suggests that the oxidation is incomplete with the low-spin Fe(IV) and high-spin(III) complexes being in rapid electron exchange on the NMR time scale. Hence, the position of the β-pyrrole resonance is likely an average isotropic shift weighted by the mole fraction of Fe(III) present.

The pH 12 spectrum in Figure 10 exhibits a β-pyrrole resonance at −1.0 ppm. Identical spectra were generated by electrolytic oxidation and by chemical oxidation with OCl$^-$ (in the form of commercial bleach) at pH 12. Upon partial oxidation by either of the above methods, both Fe(III) and Fe(IV) resonances were observed at their characteristic chemical shifts, indicating that there is *not* rapid electron exchange on the NMR time scale. The spectrum presented in Figure 10 was acquired at 76.7 MHz; however, experiments carried out at 38.4 MHz also showed separate resonances for mixtures of Fe(III) and Fe(IV). This slow electron exchange suggests that a μ-oxo dimeric intermediate is required for rapid exchange, since dimerization is unfavorable at pH 12. The oxidation is completely reversible, and the Fe(III) spectrum is regained upon reduction of the Fe(IV) complex. The ^{1}H NMR spectrum of the Fe(IV) complex does not exhibit the alternating up- and downfield aryl-proton isotropic shift signature of a porphyrin π-cation radical species derived from TPP^{2-}, and *p*-OMe-TPP^{2-} complexes have been shown to exhibit an isotropic shift signature of alternating up- and downfield shifted phenyl proton or deuteron resonances.[16a] The proton spectrum of our Fe(IV) complex shows no indication of this isotropic shift pattern (data not shown). The magnitude and direction of the Fe(IV) β-pyrrole deuteron isotropic NMR shift is consistent with previously observed β-pyrrole resonances of six-coordinate oxoiron(IV) complexes of tetraarylporphyrins.[38] Moreover, the −1.0-ppm resonance follows Curie–Weiss behavior (slope = −4234 ± 62, intercept = 13.2 ± 0.2 ppm), indicating the presence of a single species that is in a single spin state (Figure 11). Hence, the NMR spectrum is consistent with assignment of the pH 12 species as a six-coordinate oxohydroxoporphinatoiron(IV) complex, Fe^{IV}O-(2-TMPyP)(OH)$^{3+}$(aq). This assignment is consistent with the RR data presented above and with the electrochemical study by Chen et al.[2]

ESR Spectra. Figure 12 shows the ESR spectra of the Fe(I), Fe(III), and the high-valent 2-TMPyP^{2+} species. The Fe(II) complexes are ESR silent. The bottom spectra were obtained from electrolytically reduced solutions of Fe^{II}(2-TMPyP)(OH$_2$)$^{4+}$(aq) (−0.9 V at pH 9.1) and Fe^{II}(2-TMPyP)(OH)$^{3+}$(aq) (−0.88 V at pH 12.1) that were taken from the electrolysis cell and immediately frozen in quartz ESR tubes. The pH of each solution was checked following reductive electrolysis and reoxidation, and there was no change, indicating that there was no significant reduction of water due to redox cycling of the porphinatoiron complex.

The spectra of the Fe(II) reduction products are purely axial with features at g = 2.25 ($g_\perp$) and g = 1.96 ($g_\parallel$) and are typical of low-spin square-planar porphinatoiron(I) complexes.[3] The absence of any rhombic splitting of the $g_\parallel$ feature indicates that there is no mixing of the singly occupied d_{z^2} orbital with the porphyrin $\pi^*(e_g)$ orbitals and, consequently, that the complex shows no π-anion radical character.[3g] The spectra at pH 9 and 12 are superimposable, except for small peaks at g = 3.19 and g = 1.67 in the pH 12 spectrum (marked by asterisks), which may arise from a small amount of a hydroxo–Fe(I) complex. Formation of five-coordinate Fe(TPP)(py) has been demonstrated via ESR spectroscopy.[3g]

The pH 9 spectrum of Fe(III) in Figure 12 contains features that are typical of five-coordinate high-spin porphinatoiron(III) complexes (g = 5.68 and g = 2.00 (Table I)).[39] Although there is no resolvable rhombic splitting of the $g_\perp$ feature at 120 K, the fact that it deviates from a value of 6.00 indicates that $E/D \neq 0$ for at least one of the atropisomers. This is likely the result of the axially asymmetric peripheral charge distributions for the B and C atropisomers in Figure 9. The g = 2 region of the spectrum shows small contributions from some low-spin Fe(III) at 120 K that is probably due to a small fraction of the bis(hydroxo) complex that forms at low temperature.[39] The pH 12 ESR spectrum arises primarily from low-spin Fe(III) (g_z = 2.58, g_y = 2.16, and g_x = 1.87).[39] As evidenced by the feature at $g \approx 6$, however, a small fraction of the complex remains high spin, even

(38) (a) Balch, A. L.; Latos-Grazynski, L.; Renner, M. W. *J. Am. Chem. Soc.* **1985**, *107*, 2983. (b) Balch, A. L.; La Mar, G. N.; Latos-Grazynski, L.; Renner, M. W.; Thanabal, V. *J. Am. Chem. Soc.* **1985**, *107*, 3003. (c) Hickman, D. L.; Nanthankumar, A.; Goff, H. M. *J. Am. Chem. Soc.* **1988**, *110*, 6384. (d) Nanthankumar, A.; Goff, H. M. To be submitted for pubication in *Inorg. Chem.*

(39) Palmer, G. In *Iron Porphyrins, Part Two*; Lever, A. P. B., Gray, H. B., Eds.; Addison-Wesley: Reading, MA, 1983; Chapter 2.

at 120 K. The low-spin ESR parameters, Δ/λ and V/Δ,[40] for our low-spin Fe(III) complex are 8.69 and 0.43, respectively. The values indicate a relatively strong tetragonal field[6] due to the two σ- and π-donating hydroxide ligands. The low axial ligand-induced rhombicity is consistent with "type P" low-spin porphinatoiron(III) complexes, in which the axial ligand is a good π donor like thiolate,[40] or methoxide.[41]

Although the RR spectra demonstrate that the Fe(III) oxidation product is a Fe^{IV}=O complex at room temperature, the ESR spectra, taken at 120 K, are indicative of porphyrin π-cation radical species. At pH 9 (Figure 12, top) there is a broad $g = 2$ signal (line width = 430 G) and a residual $g = 6$ high-spin Fe(III) signal. The spectrum is characteristic of a π-cation radical that is efficiently relaxed by a paramagnetic metal center.[42] At pH 12 the line is even broader (2050 G) and is centered at $g = 2.44$. The deviation from $g = 2$ and the extreme width indicate appreciable coupling of the π-radical porphyrin orbital with the iron d_π orbitals.[39,42] This coupling is attributable to hydroxide binding at pH 12, since the π donor ligand would push the d_π orbital up in energy and promote mixing with the π-radical orbital. We conclude that the hole produced by oxidizing the Fe(III) complexes resides on the porphyrin at low temperature but on the iron center at room temperature.

Discussion

Iron(III). To date, only a few bis(hydroxo)porphinatoiron(III) complexes have been reported.[1,6,37,43,44] The steric and electrostatic hinderance toward μ-oxo dimer formation undoubtedly plays a role in the ability of the 2-$TMPyP^{2+}$ ligand to facilitate formation of a six-coordinate bis(hydroxo) complex. However, as illustrated by the heating experiment (Figure 8), there must be driving forces other than steric hinderance present. Our RR and magnetic resonance evidence demonstrate that this highly charged porphyrin is capable of forming a six-coordinate bis(hydroxo)iron(III) complex [Fe^{III}(2-TMPyP)$(OH)_2^{3+}$(aq)] that is thermodynamically favored over the μ-oxo dimer at pH > 11, regardless of the rotational disposition of the peripheral *N*-methylpyridyl moieties. This unique property is explained on the basis of the electron-withdrawing ability of the 2-$TMPyP^{2+}$ ligand. The ability of the peripheral positive charges to delocalize negative charge from the metal center and porphine core renders the metal ion a stronger Lewis acid than in the TPP^{2-} or TMP^{2-} complexes. Hence, the bis(hydroxide) adduct is more stable than the μ-oxo dimer. We are aware of only three other porphinatoiron(III) complexes, namely *meso*-5,10,15,20-tetrakis(2,6-difluoro)phenylporphinatoiron(III) {$Fe^{III}(TF_2PP)^+$},[43] Fe^{III}(3-$TMPyP)^{5+}$(aq),[6] and Fe^{III}(4-$TMPyP)^{5+}$(aq)[6,37,44] for which there is evidence of bis(hydroxo) formation. Interestingly, $Fe^{III}(TF_2PP)(OH)_2^-$ may also exist as a mixture of spin states at 0 °C. Whether the mixture constitutes a thermal spin state equilibrium or a quantum mechanical spin admixture is presently unknown. Although the TF_2PP^{2-} ligand has no peripheral charges the fluoro substituents render the metalloporphyrin core sufficiently electron deficient to facilitate coordination of two axial hydroxide ligands. The electrostatic argument is similar for the 4- and 3-$TMPyP^{2+}$ ligands as for the 2-$TMPyP^{2+}$ ligand. However, the attenuated electron-withdrawing ability of 4-$TMPyP^{2+}$, due to the increased distance between the positive charges and the porphyrin macrocycle, along with its increased propensity for μ-oxo dimer formation, precludes extensive formation of Fe^{III}(4-TMPyP)$(OH)_2^{3+}$(aq).[37,44]

Formation of a bis(hydroxo) complex from Fe^{III}(TMP)(OH), for which μ-oxo dimer formation is inhibited by steric hinderance alone, has not been observed.[45] However, it is possible that the solvent in which the Fe^{III}(TMP)(OH) complex was generated competes effectively at attainable OH^- concentration with the iron center by strongly solvating the hydroxide ion, thus precluding hexacoordination. A similar situation with Fe^{III}(TMP)(OMe) was circumvented by adding the strongly hydrogen-bonding fluoride ion to the solution to decrease the extent of methoxide ion solvation by excess methanol. This facilitated fluoride-assisted binding of a second methoxide ligand to generate the six-coordinate low-spin $Fe^{III}(TMP)(OMe)_2^-$ complex.[41] Since hydroxide competes effectively with fluoride ion as an axial ligand in $Fe^{III}(TF_2PP)$ complexes,[38d] this synthetic strategy could prove fruitful in generating the $Fe^{III}(TMP)(OH)_2^-$ complex.

In spite of the large positive charge of the 2-$TMPyP^{2+}$ ligand, frequencies of the porphyrin in-plane skeletal modes (Tables I and II) are similar to those for analogous high- and low-spin tetraphenylporphinatoiron(III) complexes.[12] The difference in ν_2 between the five-coordinate high-spin Fe^{III}(2-TMPyP)-$(OH)^{4+}$(aq) and $[Fe^{III}(TPP)]_2O$ complexes is only 3 cm^{-1}, with the 2-$TMPyP^{2+}$ frequency being higher. Our observation of slightly increased core frequencies for Fe^{III}(2-TMPyP) complexes relative to analogous Fe^{III}(TPP) complexes is consistent with a similar observation for the Fe^{III}(4-TMPyP) complexes.[44] The effect of the peripheral positive charges on the core sizes of the 2-$TMPyP^{2+}$ complexes is small and previously published data[12] can be used with relative confidence in predicting their core sizes.

Iron(II). The one-electron reduction product of Fe^{III}(2-$TMPyP)^{5+}$(aq) can be generated electrolytically (−0.25 V at pH 9.0 and −0.35 V at pH 12.0) or chemically via ascorbate reduction. Spectral data for the resulting Fe(II) complexes are tabulated in Tables I and II. The reduction products at pH 9 and 12 are both five-coordinate high-spin Fe(II) complexes. The β-pyrrole ^2H NMR chemical shifts are consistent with other five-coordinate high-spin tetraarylporphinatoiron(II) complexes. Finally, frequencies of the ν_2 and ν_4 bands in the Fe(II) RR spectra (see Figure 3 and Tables I and II) are consistent with those for the high-spin Fe^{II}(TPP)(2-MeIm) complex (1538, and 1341, respectively).[12] These spectral similarities suggest that the positively charged *N*-methylpyridyl groups have little effect on the orbital energies of the porphyrin macrocycle.

Table III lists the potentials of a number of Fe(III/II) couples for the indicated porphinatoiron complexes. They are less negative for 2-$TMPyP^{2+}$ than for 4-$TMPyP^{2+}$ by >0.1 V for both mono- and bis(hydroxo) complexes.[46] This effect is attributed to the greater distance between the metal ion and the peripheral charges in the 4-$TMPyP^{2+}$ derivative, which diminishes the ability of the porphyrin to stabilize the reduced metal center.

Iron(I). Further electrolytic reduction of Fe^{II}(2-$TMPyP)^{4+}$(aq) (−0.90 V at pH 9.0 and −0.88 V at pH 12.0) by one electron results in a green complex that is only sparingly soluble in aqueous perchlorate solution. In the absence of O_2, this complex is stable

Table III. Fe(III/II) Potentials for Porphinatoiron Complexes[a]

complex	$E_{1/2}$[b]	conditions	ref
Fe(TPP)$(Im)_2$Cl	−0.065	0.1 M TPAP/DMF	51
Fe(2-TMPyP)$(OH)^{4+}$	−0.075	0.1 M Na_2SO_4/H_2O, pH 9.0	2
Fe(2-TMPyP)$(OH)^{4+}$	−0.100	0.1 M $NaClO_4$, 0.1 M Na_2CO_3/H_2O, pH 9.0	c
Fe(TPP)Cl	−0.155	0.1 M TPAP/DMF	51
Fe(2-TMPyP)$(OH)_2^{3+}$	−0.225	0.2 M $NaClO_4/H_2O$, pH 12.0	c
Fe(TAP)Cl[d]	−0.241	0.1 M $LiClO_4$/DMF	3b
Fe(4-TMPyP)$(OH)^{4+}$	−0.248	0.1 N borate/H_2O, pH 9.0	46
Fe(4-TMPyP)$(OH)_2^{3+}$	−0.339	obtained from interpolation between pH 9.0 and 13 (1 N KOH)	46

[a] Potentials are reported vs Ag/AgCl. [b] Potentials are reported in volts vs the Ag/AgCl reference. These potentials have been calculated from those originally reported vs other references. [c] This work. [d] TAP = tetrakis(2-anisyl)porphyrin dianion.

(40) (a) Blumberg, W. E.; Peisach, J. *Adv. Chem. Ser.* **1971**, *No. 100*, 271. (b) Peisach, J.; Blumberg, W. E.; Adler, A. D. *Ann. N.Y. Acad. Sci.* **1973**, *206*, 310.
(41) (a) Otsuka, T.; Ohya, T.; Sato, M. *Inorg. Chem.* **1984**, *23*, 1777. (b) Otsuka, T.; Ohya, T.; Sato, M. *Inorg. Chem.* **1985**, *24*, 776.
(42) Goff, H. M.; Phillippi, M. A.; Boersma, A. D.; Hansen, A. P. In *Adv. Chem. Ser.* **1982**, *No. 201*, 357.
(43) Goff, H. M. Private communication; submitted for publication.
(44) Blom, N.; Odo, J.; Nakamoto, K.; Strommen, D. P. *J. Phys. Chem.* **1986**, *90*, 2847.
(45) Cheng, R.-J.; Latos-Grazynski, L.; Balch, A. L. *Inorg. Chem.* **1982**, *21*, 2412.
(46) Forshey, P. A.; Kuwana, T. *Inorg. Chem.* **1981**, *20*, 693.

Table IV. Fe(II/I) Potentials for Porphinatoiron Complexes[a]

complex	$E_{1/2}$[b]	conditions	ref
Fe(TPP(CN)$_4$)	−0.475	0.1 M TBAP/DMF	3g
Fe(TPP(CN)$_3$)	−0.539		3g
Fe(2-TMPyP)(OH$_2$)$^{4+}$	−0.740	0.1 M $NaClO_4$, 0.1 M Na_2CO_3/H_2O, pH 9.0	*c*
Fe(2-TMPyP)(OH$_2$)$^{4+}$	−0.755	0.1 M Na_2SO_4/H_2O, pH 9.0	2
Fe(2-TMPyP)(OH)$^{3+}$	−0.763	0.2 M $NaClO_4/H_2O$, pH 12.0	*c*
Fe(TPPBr$_4$)	−0.812	0.1 M TBAP/DMF	3g
Fe[a(Cl2)$_2$-AC][d]	−0.839	0.1 M $LiClO_4$/DMF	3b
Fe[a(Cl2)$_2$-CT][e]	−0.850		3b
Fe(TPP)	−0.986	0.1 M TBAP/DMF	3g
Fe(TPP)	−0.945		3d
Fe(TAP)[f]	−1.018	0.1 M $LiClO_4$/DMF	3b
Fe[e(Cl2)$_2$-AC][g]	−1.058		3b
Fe[e(Cl2)$_2$-CT][h]	−1.085		3b
Fe(OEP)	−1.151	0.1 M TBAP/DMF	3d

[a] Potentials are reported vs Ag/AgCl. [b] Potentials are reported in volts vs the Ag/AgCl reference. These potentials have been calculated from those originally reported vs other references. [c] This work. [d] [a-(Cl2)$_2$-AC] = adjacent-cis amide-linked C_{12} basket-handle porphyrin dianion. [e] [a(Cl2)$_2$-CT] = cross-trans amide-linked C_{12} basket-handle porphyrin dianion. [f] TAP = tetrakis(2-anisyl)porphyrin dianion. [g] [e-(Cl2)$_2$-AC] = adjacent-cis ether-linked C_{12} basket-handle porphyrin dianion. [h] [e(Cl2)$_2$-CT] = cross-trans ether-linked C_{12} basket-handle porphyrin dianion.

for many hours at room temperature. The extra electron resides on the Fe(I) center, which is low spin, as shown by the RR core size frequencies and by the ESR spectra. In a study of tetraarylporphinatoiron(II) complexes with different electron-withdrawing abilities, Donohoe et al.[3g] showed that if there is mixing of the d_π orbitals of the metal ion and the porphyin π^* orbitals, the ESR **g** tensor looses its tetragonal symmetry and becomes rhombic. This was the case for Fe(TPPBr$_4$)$^-$ for which $g_x = 2.39$, $g_y = 2.16$, and $g_z = 1.94$. Substitution of cyano groups on the β-pyrrole carbons in [Fe(TPP)CN)$_4$)$^-$] pushes the porphyrin π^* orbitals even further down in energy and the ESR spectrum of the low-valent complex collapsed into a single asymmetric line centered at $g = 2$, indicating nearly pure porphyrin radical anion character of the HOMO in the reduced complex. The ESR spectra of our reduced complexes at pH 9 and 12 (Figure 12) are clearly axial and arise from square-planar Fe(I) species.

Table IV lists the Fe(II/I) potentials for a number of porphinatoiron complexes. It shows that, with the exception of the cyanoporphyrins, the Fe(II/I) potentials for the aqueous 2-TMPyP^{2+} complexes are among the least negative of any yet reported. This is interesting, because the complexes above and below the 2-TMPyP^{2+} complexes in Table IV both exhibit mixing of the porphyrin π^* and metal d_π orbitals.[3g] The fact that the 2-TMPyP^{2+} complexes exhibit no anion radical character indicates that the peripheral positive charges do not significantly perrturb the porphyrin π^* energy levels, probably because the pyridyl rings are nearly perpendicular to (or at least, not coplanar with) the porphyrin macrocycle and are not directly involved in π delocalization pathways. Thus, the *N*-methyl groups are able to stabilize the low valent metal ion via an electrostatic interaction that does not significantly perturb the interactions between the porphyrin π^* and metal d orbitals relative to those of the TPP^{2-} complex.

Iron(IV). On the basis of the arguments presented above for the ability of 2-TMPyP^{2+} to stabilize low oxidation states of iron, it might seem reasonable to predict a destabilization of high-valent states. In fact, quite the opposite is observed. As the solution pH is raised, the stability of the Fe(IV) species becomes greater due to coordination of a hydroxide ligand in the axial position trans to the ferryl oxygen.

The Fe(IV/III) potential for the 2-TMPyP^{2+} complex at pH 12 is substantially lower than those reported to date for Fe^{III}–OH or Fe^{III}–OCH$_3$ porphyrin complexes (Table V).[10,47,48] We attribute this lowering to stabilization of the Fe^{IV}=O unit by coordination of a trans hydroxide ligand. Hydroxide binding is favored by the positively charged porphyrin and by the aqueous alkaline medium (the other iron(IV/III) porphyrin potentials refer to methylene chloride solutions with a small amount of dissolved base).

Table V. Fe(IV/III) Potentials for Porphinatoiron Complexes[a]

complex	$E_{1/2}$[b]	conditions	ref
Fe(2-TMPyP)(OH)$^{4+}$	+0.645	0.1 M Na_2SO_4/H_2O, pH 9.0	2
Fe(2-TMPyP)(OH)$_2^{3+}$	+0.709[c,d]	0.2 M $NaClO_4/H_2O$, pH 12.0	*e*
Fe(2-TMPyP)(OH)$^{4+}$	+0.78[c]	0.1 M $NaClO_4$, 0.1 M Na_2CO_3/H_2O, pH 9.0	*e*
Fe(TTMPP)(OH)[f]	+0.905	0.1 M TBAP/CH_2Cl_2	47
Fe(TPP)(OCH$_3$)	+1.155		47
Fe(TMP)(OCH$_3$)	+1.055		10, 47
Fe(TMP)(OH)	+1.055		48
Fe(TMP)(OH)	+1.045		10
Fe(TDCPP)(OCH$_3$)[g]	+1.305		47
Fe(TDCPP)(OH)	+1.305		47
Fe(TDFPP)(OCH$_3$)[h]	+1.425		47
Fe(TDFPP)(OH)	+1.425		47

[a] Potentials are reported vs Ag/AgCl. [b] Potentials are reported in volts vs the Ag/AgCl reference. These potentials have been recalculated from those originally reported vs other references. [c] Irreversible wave; potential reported is the potential of the anodic wave at a scan rate of 50 mV/s. [d] $E_{1/2}$ is estimated to be 0.65 ± 0.02 V on the basis of a very small cathodic wave. [e] This work. [f] TTMPP = tetrakis(2,4,6-trimethoxyphenyl)porphyrin dianion. [g] TDCPP = tetrakis(2,6-dichlorphenyl)porphyrin dianion. [h] TDFPP = tetrakis(2,6-difluorophenyl)porphyrin dianion.

Table VI. Calculated Fe–OH Force Constants

complex	spin state	ν_{Fe-OH} (cm^{-1})	force constant[a] (mdyn/Å)	ref
Fe^{II}(2-TMPyP)(OH)$^{3+}_{(aq)}$	HS	463	1.65	*b*
Fe^{III}(2-TMPyP)(OH)$^{4+}_{(aq)}$	HS	541	2.25	1a
Fe^{III}(2-TMPyP)(OH)$_2^{3+}_{(aq)}$	HS	447[c]	2.00	1b
Fe^{III}(2-TMPyP)(OH)$_2^{3+}_{(aq)}$	LS	498[c]	2.48	1b

[a] Calculated using point masses of 56 amu for Fe and 17 amu for the OH^- ligand, using a diatomic oscillator approximation for the Fe(OH) complexes and a linear triatomic oscillator approximation for the Fe(OH)$_2$ complexes. The latter approximation actually yields a symmetry force constant which is the sum of the valence force constant and the interaction force constant between the Fe–OH stretches. [b] This work. [c] Frequency of symmetric HO–Fe^{III}–OH stretch.

Hydroxide binding is the basis for the low Fe^{IV}=O stretching frequency, 763 cm^{-1}, for the pH 12 oxidation product. Interestingly, a 818-cm^{-1} band has been detected for the oxidation product of Fe^{III}(4-TMPyP)(OH)$^{4+}$(aq) at pH 9.4, which is stable for a few minutes at room temperature.[4b] This frequency is mid-way between 763 cm^{-1} and the value observed for the five-coordinate ferryl porphyrins Fe^{IV}O(TMP)[24] and Fe^{IV}O(TPP),[23] 840 and 850 cm^{-1}, respectively. We infer that at pH 9.4 the 4-TMPyP^{2+} ferryl species has a trans OH_2 ligand, whose donor strength is substantially less than that of hydroxide. The situation is entirely analogous to the previously characterized vanadyl porphyrins; the V^{IV}=O frequency is seen at 996 cm^{-1} for five-coordinate VO(TPP), but 955 cm^{-1} for aqueous VO(4-TMPyP)(OH$_2$)$^{4+}$(aq) and 895 cm^{-1} for VO(4-TMPyP)-(OH)$^{3+}$(aq) at pH 14.[22]

Fe–OH Force Constants. The detection of Fe–OH stretching frequencies for Fe(II) and for high- and low-spin iron(III) hydroxide complexes of 2-TMPyP^{2+} provides a unique opportunity to compare Fe–OH bond strengths as a function of oxidation and spin state of the iron. Table VI lists the frequencies and force constants calculated for the Fe(II) and Fe(III) complexes of 2-TMPyP^{2+}. Comparing five-coordinate high-spin Fe(II) and Fe(III) complexes, we see that, as expected, the force constant is much higher for Fe(III) (2.25 vs 1.65 mdyn/Å). Since the

(47) Lee, W. A.; Calderwood, T. S.; Bruice, T. C. *Proc. Natl. Acad. Sci. U.S.A.* **1985**, *82*, 4301.

(48) Calderwood, T. S.; Bruice, T. C. *Inorg. Chem.* **1986**, *25*, 3722.

electronic configuration differs only by an additional d_π nonbonding electron in high-spin Fe(II), the difference is attributable mainly to the increased nuclear charge on Fe(III). On the basis of Badger's rule,[49] we estimate the decrease in the Fe–OH distance to be 0.124 Å, as expected from the difference in the Fe^{2+} and Fe^{3+} ionic radii (0.135 Å).[50]

When a second OH^- is bound to the high-spin Fe(III) complex, the force constant drops from 2.25 to 2.00 mdyn/Å. (Strictly speaking, the latter value is the sum of the principal force constant and the interaction force constant between the two Fe–OH stretches.) This trans effect is due to the competition between the two OH^- ligands for the Fe(III) bonding orbital, d_{z^2}. The removal of the unpaired electron from this orbital in the low-spin $Fe^{III}(OH)_2$ complex accounts for the increase in the force constant from 2.00 to 2.48 mdyn/Å. Badger's rule gives 0.046 Å for the corresponding decrease in the bond distance, a value that is smaller than the ~0.1 Å difference expected between high- and low-spin Fe(III) complexes.[50] The decrease in the Fe–OH distance brought about by the enhanced σ-interaction is counteracted by the strong π donor properties of the hydroxide ligands. The OH^- π orbitals interact in an antibonding fashion with the partially filled Fe d_π orbitals. This resulting lengthening of the Fe–OH bond might account for the ν_2 core size marker frequency being 14 cm^{-1} higher for low-spin $Fe^{III}(2\text{-}TMPyP)(OH)_2^{3+}(aq)$ than for the low-spin imidazole adduct $Fe^{III}(TPP)(ImH)_2Cl$.[12] The nonbonded repulsions between the pyrrole-N atoms and the axial ligand may be weaker for OH^- than for ImH, allowing the porphyrins to contract.

(49) (a) Badger, R. M. *J. Chem. Phys.* **1934**, *2*, 128. (b) Badger, R. M. *J. Chem. Phys.* **1935**, *3*, 710. (c) Herschbach, D. R.; Laurie, V. W. *J. Chem. Phys.* **1961**, *5*, 458.
(50) Shannon, R. D.; Prewitt, C. T. *Acta Crystallogr.* **1969**, *B25*, 925.
(51) Felton, R. H. In *The Porphyrins*; Dolphin, D., Ed., Academic Press: New York, 1978; Vol. 5, Chapter 3.

Conclusions

The 2-$TMPyP^{2+}$ ligand shows a remarkable ability to stabilize high and low metalloporphyrin oxidation states via control of ligation environment and of molecular charge. We have demonstrated that in the presence of 10^{-2} to 10^{-1} M hydroxide ion the Fe(I), Fe(II), Fe(III), and Fe(IV) complexes of 2-$TMPyP^{2+}$ can be generated via chemical and/or electrochemical means. These complexes are stable at ambient temperature for relatively long periods of time. This stability is remarkable in light of the fact that numerous earlier porphinatoiron(I) and iron(IV) studies have been *plagued* by the presence of trace amounts of water. The Fe(I) stability is based in the ability of the positively charged porphyrin ligand to delocalize electron density from the metal ion via a primarily electrostatic mechanism. In high oxidation states, this same electrostatic influence of the porphyrin ligand results in a high affinity of the metal center for axial ligands. Thus the Fe^{IV}=O complex binds hydroxide and thereby gains thermodynamic and kinetic stability relative to five-coordinate oxoporphinatoiron(IV) complexes. The Fe^{IV}=O stretching frequency has been identified at 763 cm^{-1} and is consistent with axial coordination by a hydroxide ligand trans to the ferryl oxygen.

In summary, the stabilization effects exhibited by this ligand are largely electrostatic in nature and not due to perturbations of the porphine core molecular orbital energies. This has important implications in the design and tailoring of transition metal reagents and catalysts for effecting useful oxidation and reduction chemistry. Moreover, it further illustrates the latitude that nature has at her disposal to "tune" heme reactivity via variations in the electrostatic potential around the prosthetic sites in heme proteins.

Acknowledgment. This work was supported by U.S. Department of Energy Grant DEFG02-88ER13876 (T.G.S.) and the National Science Council of the Republic of China (Y.O.S.). K.R.R. (1 F32 HL08116-01) and R.A.R. (GM12197-02) are recipients of NIH National Research Service Awards.

Contribution from the Department of Chemistry, University of Missouri—St. Louis, 8001 Natural Bridge Road, St. Louis, Missouri 63121

Kinetics of Iron Removal from Monoferric and Cobalt-Labeled Monoferric Transferrins by Diethylenetriaminepenta(methylenephosphonic acid) and Diethylenetriaminepentaacetic Acid

Wesley R. Harris,*,† Pawan K. Bali,‡ and Michael M. Crowley†

Received July 24, 1991

Rate constants for the removal of ferric ion from transferrin by the octadentate chelating agents diethylenetriaminepenta(methylenephosphonic acid) (DTPP) and diethylenetriaminepentaacetic acid (DTPA) have been measured for both N- and C-terminal monoferric transferrin in 0.1 M *N*-(2-hydroxyethyl)piperazine-*N'*-2-ehtanesulfonic acid buffer at pH 7.4 and 25 °C. Iron removal by the amino carboxylate DTPA appears to follow simple first-order kinetics. However, plots of the observed pseudo-first-order rate constant for iron removal versus the concentration of DTPP follow neither simple first-order nor saturation kinetics. The results on DTPP are interpreted in terms of two parallel pathways for iron removal, one which shows saturation kinetics and another which is first order in DTPP. The site preferences for the two ligands are also different. While DTPA preferentially removes iron from the N-terminal site, DTPP preferentially removes ferric ion from the thermodynamically more stable C-terminal binding site. Labeling the vacant binding sites of the monoferric transferrins with kinetically inert cobalt(III) has little effect on the rates of iron removal by DTPP. Equilibrium constants for the binding of the anionic DTPP ligand to the apoprotein have also been determined. The successive macroscopic binding constants are log K_1 = 6.25 ± 0.16 and log K_2 = 4.68 ± 0.17.

Introduction

Transferrin is a serum protein whose primary function is to transport ferric ion among sites of uptake, utilization, and storage.[1-4] The distinguishing characteristic of the transferrins is the requirement of concomitant binding of a synergistic anion to form a stable metal–transferrin complex. Under biological conditions, bicarbonate is the synergistic anion, although a variety of other anions will form weak Fe–L–Tf complexes under bi-

† University of Missouri—St. Louis.
‡ Present address: Department of Physiology and Biophysics, Albert Einstein College of Medicine, Bronx, NY 10461.

(1) Harris, D. C.; Aisen, P. In *Iron Carriers and Iron Proteins*; Loehr, T. M., Ed.; VCH Publishers: New York, 1989; pp 239-352.
(2) Aisen, P. In *Iron Carriers and Iron Proteins*; Loehr, T. M., Ed.; VCH Publishers: New York, 1989; pp 353-372.
(3) Brock, J. H. In *Metalloproteins*; Harrison, P., Ed.; Macmillan: London, 1985; Part II, pp 183-262.
(4) Bates, G. W.; Graybill, G.; Chidambaram, M. V. In *Control of Animal Cell Proliferation*; Boynton, A. L., Leffert, H. L., Eds.; Academic Press: New York, 1987; Vol. II, pp 153-202.

0020-1669/92/1331-2700$03.00/0